Máster Universitario en Astrofísica

Universidad Complutense de Madrid

Trabajo de Fin de Máster

CARMENES target characterisation: mining public archives for high-resolution spectra of M dwarfs with exoplanets

---

Alumno:
Héctor Martínez Rodríguez [I]

Directores:
David Montes [II] (UCM), José Antonio Caballero [III] (CAB)

Tutor:
David Montes [II] (UCM)

Julio 2014

[I] h.martinez@ucm.es
[II] dmontes@ucm.es
[III] caballero@cab.inta-csic.es

Resumen:

Contexto: CARMENES es un espectrógrafo de alta resolución con el que el consorcio hispano-alemán del mismo nombre buscará exotierras alrededor de unas 300 estrellas enanas de tipo espectral M por el método de velocidad radial.
Objetivos: La caracterización espectral del máximo numero de estrellas posible será esencial para descubrir enanas M candidatas a albergar exoplanetas y, por tanto, para refinar la muestra antes de que el proyecto CARMENES salga a la luz. Por consiguiente, deseamos ayudar al consorcio internacional a completar la base de datos CARMENCITA con espectros de alta resolución de enanas M de la base de datos de la ESO.
Métodos: Se han recopilado 128 espectros de UVES pertenecientes a 61 estrellas de la base de datos CARMENCITA, cuyo estudio se ha llevado a cabo mediante el entorno IRAF. Se ha cubierto el rango de longitudes de onda 3250–10500 Å con un total de ocho canales distintos.
Resultados: Hemos calculado las pseudoanchuras equivalentes de las líneas H & K del Ca II, D_3 del He I, del doblete D_1 & D_2 del Na I y de las líneas de la serie de Balmer Hα, Hβ, Hγ, Hδ, Hη y Hζ. Esto nos ha permitido hallar tanto estrellas de baja actividad como de alta actividad. Por otro lado, también hemos calculado velocidades de rotación.
Conclusiones: Nuestro estudio ha permitido clasificar las estrellas en función de su actividad cromosférica, íntimamente relacionada con las líneas de absorción y emisión y con la velocidad de rotación. Las estrellas poco activas son especialmente interesantes para CARMENES debido a su baja velocidad de rotación.

Palabras clave: Bases de datos astronómicas — Estrellas: actividad — Estrellas: tipo tardío — Estrellas: baja masa — Estrellas: rotación — Galaxia: vecindad

Abstract:

Context: CARMENES is a next-generation instrument being built by a consortium of German and Spanish institutions to carry out a survey of 300 M-type dwarf stars with the goal of detecting exoearths by radial-velocity measurements.
Aims: The spectral characterisation of the maximum possible number of stars will be essential to discover M dwarfs that are candidates to host exoplanets and, hence, to refine the sample before CARMENES comes to light. Hence, we want to help the international consortium to complete CARMENCITA database with high-resolution spectra of M dwarfs from the ESO database.
Methods: We have compiled 128 UVES spectra belonging to 61 stars from CARMENCITA database, which study has been carried out with the environment IRAF. We have covered the wavelength range 3250–10500 Å with a total of eight different channels.
Results: We have calculated the pseudo-equivalent widths of Ca II H & K lines, He I D_3 line, Na I doublet D_1 & D_2 lines and Balmer series lines Hα, Hβ, Hγ, Hδ, Hη and Hζ. This has allowed us to find both low-activity and high-activity stars. On the other hand, we have also calculated rotational velocities.
Conclusions: Our study has allowed to classify the stars according to their chromospheric activity, closely related to absorption and emission lines and rotational velocity. Low-activity stars are specially interesting to CARMENES because of their low rotational velocity.

Keywords: Astronomical data bases — Stars: activity — Stars: late-type — Stars: low-mass — Stars: rotation — Galaxy: neighbourhood

Index

1 Introduction **3**
1.1 M dwarfs . . . 3
1.1.1 High-resolution spectroscopy of M dwarfs . . . 4
1.1.2 Stellar chromospheric activity . . . 5
1.2 High-resolution spectrographs . . . 6
1.2.1 HARPS . . . 6
1.2.2 UVES . . . 7
1.2.3 Other spectrographs . . . 7

2 Analysis **9**
2.1 Spectra compilation . . . 9
2.2 Spectra . . . 12
2.3 Pseudo-equivalent widths . . . 14
2.4 $H\alpha$ line measurements . . . 16
2.5 Rotational velocities . . . 17

3 Results and discussion **21**
3.1 pEWs vs $pEW(H\alpha)$ . . . 21
3.2 pEWs vs spectrals types . . . 22
3.3 Flares . . . 23
3.4 Obtained values of $v \sin i$ . . . 23
3.5 pEWs(Hα) vs rotational velocities . . . 24

4 Conclusions and future research **25**

Appendix: Figures **27**

Appendix: Tables **32**

1 Introduction

1.1 M dwarfs

M dwarfs represent around 66 % of the total stellar mass of our Milky Way and about 33% of the main-sequence stars in the solar neighbourhood (Reid et al. 1995; Hawley et al. 1996). They are not bright enough to be visible with the unaided eye, but their study is quite relevant to understand the galactic structure and star formation.

In the context of the spectral taxonomy developed at Harvard University in the 1890s according to the strength of hydrogen absorption lines, M dwarfs are the coolest (late-type) stars. Although most M stars are red dwarfs, this class also hosts giants and supergiants and, furthermore, late-M stars hold very young brown dwarfs, objects with too little mass to allow nuclear reactions to occur in their interiors but deuterium burning. Typical characteristics of M dwarfs are shown in Table 1:

Table 1: M dwarfs typical characteristics (Reid & Hawley 2005).

Spectral type (SpT)	M0V	M1V	M2V	M3V	M4V	M5V	M6V	M7V	M8V	M9V
Mass [$M_\odot$]	0.6	0.49	0.44	0.36	0.20	0.14	0.10	0.09	0.08	0.075
Radius [$R_\odot$]	0.62	0.49	0.44	0.39	0.26	0.20	0.15	0.12	0.11	0.08
Luminosity [10^{-3} $L_\odot$]	72	35	23	15	5.5	2.2	0.9	0.5	0.3	0.15
log g [cgs]	4.65	4.75	4.8	4.8	4.9	5.0	5.1	5.2	5.2	5.4
$T_{\rm eff}$ [K]	3800	3600	3400	3250	3100	2800	2600	2500	2400	2300

M dwarfs are very cool, little and low-mass stars. In general, most M dwarfs are fully convective due to their high opacity, as partially ionized hydrogen zones increase the electron density. Besides, Rayleigh diffusion ans molecular absorptions have an essential role in opacity. Convective zones arise in F2V stars alongside radiative energy transport, while M4V and later-type stars are completely convective. M dwarfs are located in the lowest part of the main sequence. They are, in general, Population I stars, i.e., they are rich in metals and hence present plenty of molecular bands in their spectra. Employing Wien's law, their peak of emission is located around $\sim$ 0.7–1.4 μm. Thus, M dwarfs spectra will present a poor signal-to-noise ratio in the near ultraviolet and a good quality in the optical and near infrared.

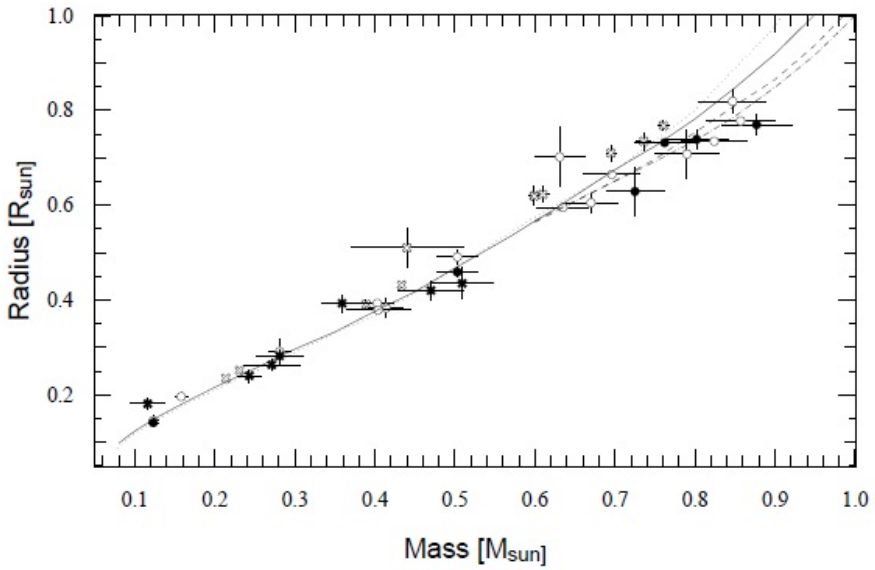

Figure 1: Mass-radius relation of low and very low-mass stars revisited with the VLTI (Demory et al. 2009).

1.1.1 High-resolution spectroscopy of M dwarfs

Spectroscopy is, along with photometry, a fundamental technique in astrophysics. *Grosso modo*, it consists of dispersing the light according to its wavelength with instruments called spectrographs. If we denote by $\delta\lambda$ the spectral purity of the instrument, Rayleigh criterion for resolution asserts that a line of width $\Delta\lambda$ is resolved if

$$\delta\lambda < \Delta\lambda$$

Then, the resolving power of a spectrograph is given by $R = \lambda/\delta\lambda$, which allows us to distinguish between low ($R \sim 10^3$), intermediate ($R \sim 10^4$) and high-resolution spectroscopy ($R \geq 5 \times 10^4$). We are clearly interested in high-resolution spectra (see section 2), obtained thanks to echelle spectrographs, diffraction gratings characterised by a relatively low groove density but a groove shape that is optimized for use at a high incidence angle and therefore in high diffraction orders.

Let's talk about stellar spectra. A spectrum is a graphic that shows the observed flux as a function of the wavelength. It presents different characteristics:

- Continuum spectrum. Interactions between matter and radiation in the interior of a star produce a constant flux (local thermodynamic equilibrium). Absorption and emission lines are superposed to this continuum.
- Absorption lines. Formed in the photosphere, the surface layer that emits the radiation we observe photometrically and spectroscopically (usually called "stellar atmosphere", negative gradient of temperature). They consist of a flux deficiency in comparison with the expected from a radiative equilibrium atmosphere. The less intense these lines are, the deeper are the layers where they are formed.
- Emission lines. Formed in the chromosphere (positive gradient of temperature), a layer placed above the photosphere. They consist of a flux excess in comparison with the expected from a radiative equilibrium atmosphere.
- Molecular bands. Essential feature of late-type stars. Due to their low temperatures, molecular transitions are predominant and molecular bands (which overlap) appear all over a wide range, usually beginning around 6000 Å. Titanium oxide absorption bands are the defining characteristic of M stars.

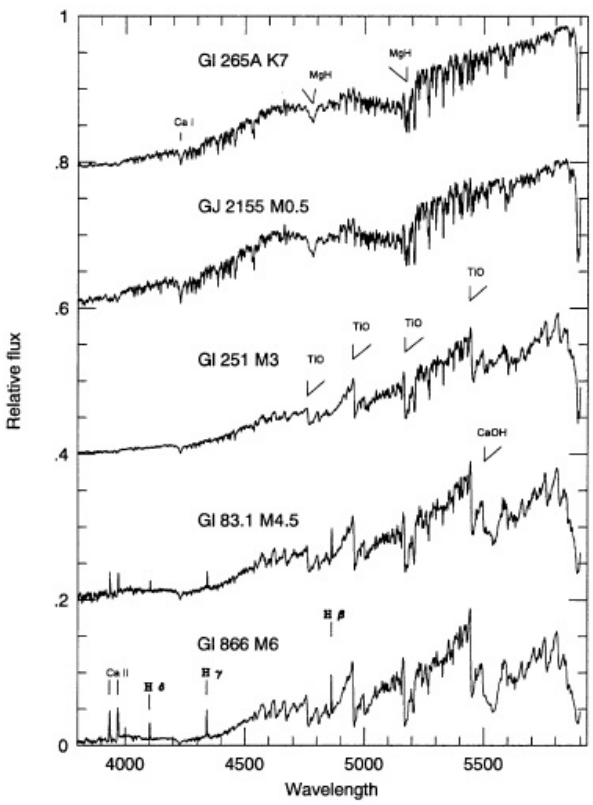

(a) Blue optical spectra of M dwarfs.

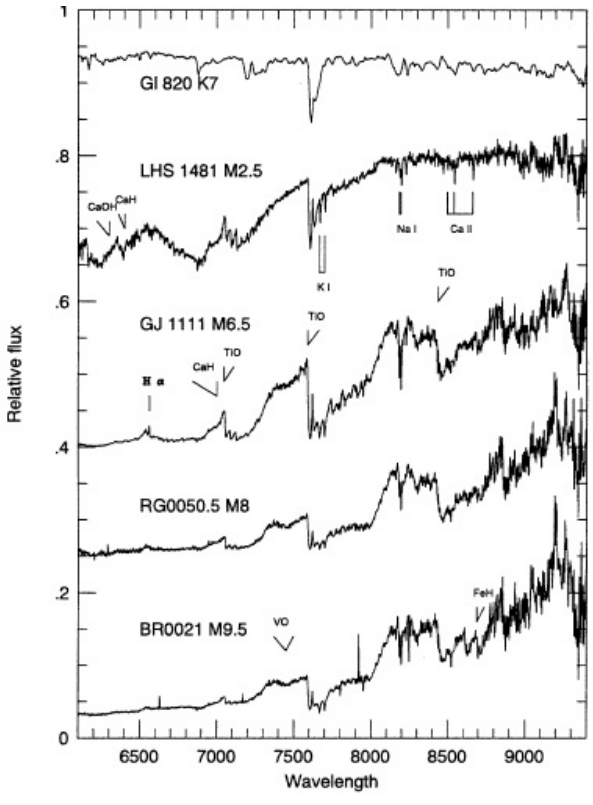

(b) Red optical spectra of M dwarfs.

Figure 2: Optical spectra of M dwarfs (Reid & Hawley 2005).

Figs. 2a and 2b present optical spectra of representative K and M dwarfs, identifying the principal spectral features. TiO is present, but weak, at type K7, and grows in strength until type M6, where most of the bandheads saturate. Bands due to several metal hydrides (MgH, FeH and CaH) also first become detectable among K7 stars and grow in prominence with later spectral type.

However, it must be noted that, because of these bands, *it is not possible to define a continuum for M dwarfs*. Whenever they appear spectra elevate and are not plain at all. Furthermore, M stars present plenty of absorption lines in the "plain" region that variate the continuum height, so we talk about *pseudocontinuum*. We know that the equivalent width of a line is the width of a rectangle which height is the one of the continuum and which area is the one enclosed by the line:

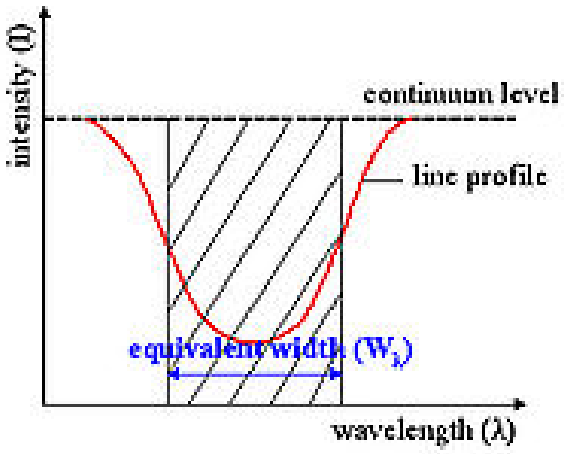

Figure 3: Concept of equivalent width.

Hence, we must introduce the concept of *pseudo-equivalent width* (from now on pEW). Its definition is identical to the one of the equivalent width, just considering the pseudocontinuum instead of the continuum.

1.1.2 Stellar chromospheric activity

Most M stars in the galactic disk appear to maintain nearly constant photometric properties. However, a subset exhibits high stellar chromospheric activity, which is tied to the structure of the subsurface convection zone, to a high rotation and to changes in a strong shallow magnetic field that is regenerated via a self-sustaining dynamo. Regarding stellar spectra, activity is manifested as strong emission peaks, which completely overshadow the absorption lines formed in the photosphere. High-activity stars may present substantial and short-term luminosity variations called *flares*, phenomena we will study in subsection 3.3.

We indicate several spectral lines that are good indicators of stellar chromospheric activity when they appear as strong emission peaks:

- Balmer series: Hα, Hβ, Hγ and Hδ.
- Mg II h & k.
- Ca II H & K (strongest spectral features of activity).
- Ca I at 4226 Å.
- Na I D_1 & D_2.
- He I D_3.
- Ca II IRT (infrared triplet).

Balmer series lines (electron transition from $n \geq 3$ to $n = 2$) are essential in astrophysics because they appear in numerous stellar objects due to the high abundance of hydrogen in the Universe. Furthermore, they are commonly seen and relatively strong compared to lines from other elements. We know that the wavelengths λ of Balmer series absorption/emission lines are given by the following formula:

$$\frac{1}{\lambda} = R_H \left(\frac{1}{2^2} - \frac{1}{n^2} \right)$$

where $R_H = 1.097 \cdot 10^7\ m^{-1}$ is the Rydberg constant for hydrogen. We show some values of these wavelengths:

Table 2: Balmer series.

Line	Hα	Hβ	Hγ	Hδ	Hϵ	Hζ	Hη	H8	H9	H10
λ [Å]	6563.0	4861.5	4340.6	4101.9	3970.2	3889.2	3835.5	3798.0	3770.8	3750.3

Line	H11	H12	H13	H14	H15	H16	H17	H18	H19	H20
λ [Å]	3734.5	3722.1	3712.1	3704.0	3697.3	3691.7	3687.0	3682.9	3679.5	3676.5

So the first and main lines essentially appear in the visual range. He I and Na I lines are well-known, while Ca II H & K lines appear next to the lower limit of the visual range. To conclude this subsection we show all the spectral lines we have considered in our study:

Table 3: Studied spectral lines.

Line	Hη	Hζ	Ca II K	Ca II H	Hϵ	Hδ	Hγ	Hβ	He I D_3	Na I D_2	Na I D_1	Hα
$\lambda[Å]$	3835.5	3889.2	3933.7	3968.5	3970.2	4101.9	4340.6	4861.5	5875.7	5890.0	5896.0	6563.0

1.2 High-resolution spectrographs

1.2.1 HARPS

HARPS[IV] (High Accuracy Radial velocity Planet Searcher) is the ESO facility for the measurement of radial velocities with the highest accuracy currently available. It is fibre-fed by the Cassegrain focus of the 3.6 m telescope in La Silla.

The instrument is built to obtain very high long term radial velocity accuracy (on the order of 1 m/s). To achieve this goal, HARPS is designed as an échelle spectrograph fed by a pair of fibres and optimised for mechanical stability. It is contained in a vacuum vessel to avoid spectral drift due to temperature and air pressure variations. One of the two fibres collects the star light, while the second is used to either record simultaneously a Th-Ar reference spectrum or the background sky. The two HARPS fibres (object + sky or Th-Ar) have an aperture on the sky of 1 arcsec, which produces a resolving power of 115,000 in the spectrograph. Both fibres are equipped with an image scrambler to provide a uniform spectrograph pupil illumination. The spectral range covered is 378–691 nm, distributed over the échelle orders 89–161. As the detector consists of a mosaic of 2 CCDs (altogether 4k x 4k, 15 μm pixels), one spectral order (N=115, from 530 nm to 533 nm) is lost in the gap between the two chips.

HARPS is equipped with its own pipeline (installed at La Silla), which provides the visiting astronomer in near real-time with extracted and wavelength calibrated spectra in all observing modes. When the simultaneous reference method is applied, the pipeline delivers precise radial velocities (RV, relative to the solar system barycentre) for late type stars whose RV is known within 1 - 2 km/s, provided that a set of standard calibrations has been executed in the afternoon.

[IV] http://www.eso.org/sci/facilities/lasilla/instruments/harps.html

On the other hand, we must mention that the HARPS-North spectrograph is a high-precision radial-velocity instrument, similar to HARPS on the 3.6-m ESO telescope in Chile. Located in the Northern hemisphere and installed at the TNG on La Palma Island (Canary Islands) to allow for synergy with the NASA Kepler mission. Its main scientific rationale is the characterization and discovery of terrestrial planets by combining transits and Doppler measurements.

1.2.2 UVES

UVES[V] (Ultraviolet and Visual Echelle Spectrograph) is the high-resolution optical spectrograph of the VLT located at the Nasmyth B focus of UT2 (Cerro Paranal). It is a cross-dispersed échelle spectrograph designed to operate with high efficiency from the atmospheric cut-off at 300 nm to the long wavelength limit of the CCD detectors (about 1100 nm). To this aim, the light beam from the telescope is split in two arms (UV to Blue, and Visual to Red) within the instrument. The two arms can be operated separately or in parallel via a dichroic beam splitter.

UVES resolving power is about 40,000 when a 1-arcsec slit is used, and the maximum (two-pixel) resolution is 80,000 or 110,000 in the Blue and the Red Arm, respectively. Three image slicers are also available to obtain high resolving power without excessive slit loss. The instrument is built for maximum mechanical stability and allows for accurate wavelength calibration. An iodine cell can be inserted in the light beam for observations requiring extremely high accuracy for radial velocity measurements.

Table 4: UVES spectroscopic modes.

Instrument mode	Accessible $\Delta\lambda$ (nm)	Maximum R ($\lambda/\Delta\lambda \times 10^3$)	Covered $\Delta\lambda$ (nm)	Magnitude limits
Blue arm	300-500	80	80	17-18
Red arm	420-1100	110	200-400	18-19
Dichroic #1	300-400	80	80	17-18
	500-1100	110	200	18-19
Dichroic #2	300-500	80	80	17-18
	600-1100	110	400	18-19
Iodine cell	500-600	110	200	17

The magnitude limits listed above are estimated on the basis of the following conditions: continuum source, 0.7 arcsec seeing, 1 arcsecslit, no binning, 3-hour integration time, S/N of 10 (per resolution element) at the peak of the central order, no moon. They are indicative of the limiting performance of the instrument only as they depend on the wavelength. S/N accurate estimates require the use of the Exposure Time Calculator.

1.2.3 Other spectrographs

Of course, there are much more high-resolution spectrographs. We briefly mention some of them:

- Near infrared.
  - CRIRES (High Accuracy Radial velocity Planet Searcher) is a cryogenic high-resolution infrared échelle spectrograph located at the Nasmyth focus A of UT1 (Antu). It provides a resolving power of up to 100,000 between 0.95 and 5.38 μm and is housed in a vacuum vessel, with its optics cooled to $\sim$ 65 K and the detectors to $\sim$ 25 K. CRIRES will be removed in July 2014 for an upgrade, while it is expected that CRIRES+ will be back in operations during 2017.
  - GIANO is an optimized near infrared échelle spectrograph that can yield, in a single exposure, 0.9–2.5 mm spectra at a resolution R$\sim$50,000. This project is part of the Second Generation Instrumentation Plan of the Telescopio Nazionale Galileo (TNG) located at Roque de Los Muchachos Observatory (ORM), La Palma, Spain and it has been entirely funded by the Istituto Nazionale di Astrofisica (INAF). GIANO can

[V] http://www.eso.org/sci/facilities/paranal/instruments/uves.html

provide high resolution spectra for accurate radial velocity measurements of exoplanets and for chemical and dynamical studies of stellar or extragalactic objects down to a magnitude limit comparable to that of 2MASS.

- SPIRou is a near-infrared spectropolarimeter and high-precision velocimeter being designed as a new Guest Instrument for Canada-France-Hawaii Telescope (CFHT) located atop the summit of Mauna Kea. It will be installed at the Cassegrain telescope focus in 2017 after its construction and validation tests are performed by the instrument consortium. The main science goals of SPIRou are the search and characterization of habitable exo-Earths around low-mass stars and the study of the magnetic topology of young protostars as a tool for investigating star/planet formation mechanisms.
- HPF (Habitable Zone Planet Finder) is an astronomical spectrograph currently in development that will be installed on the 10 m Hobby-Eberly Telescope at McDonald Observatory in Texas. HPF will be placed in a vacuum chamber cooled to 180 K and will search for nearby small exoplanets around M dwarfs.

- Visible.

  - FEROS (Fiber-fed Extended Range Optical Spectrograph) is a state-of-the-art bench-mounted, high-resolution, environmentally controlled, astronomical échelle spectrograph. It is located in La Silla (Chile). Its high efficiency (20%), large wavelength range (the complete optical spectral region in one exposure) and high resolution (R=48,000) makes possible a large variety of stellar and extra-galactic spectroscopic observation programs requiring high spectral stability.
  - PFS (The Carnegie Planet Finder Spectrograph) is a high resolution, optical échelle spectrograph that covers wavelengths from 388 to 668 nm with resolving powers from 38,000 to 190,000. It is hard at work searching for extrasolar planets with the the 6.5 m Magellan II Telescope at Las Campanas Observatory in Chile. It detects exoplanets through their gravitational influence on their host stars, which cause Doppler shifts in the stellar spectra that can be measured to give the stellar velocities to a precision better than 1 m/s. As the planets orbit their hosts, the measured stellar velocities vary periodically, revealing the planetary presence and information about their masses and orbits.
  - CAFE (Calar Alto Fiber-fed Échelle spectrograph) is an instrument constructed at CAHA to replace FOCES, the high-resolution échelle spectrograph at the 2.2 m Telescope of the observatory.
  - ESPRESSO (Échelle SPectrograph for Rocky Exoplanet- and Stable Spectroscopic Observations) is a new-generation spectrograph for ESO's VLT. The amazing spectroscopic precision of this instrument will provide the community with new scientific capabilities that are unique world-wide. In particular, the ESPRESSO Consortium will invest the Guaranteed-Time Observation (GTO), awarded in return to the major investment, into two major scientific programmes: the search for rocky extra-solar planets in the habitable zone of their host stars and the determination of the possible variability of physical constants. It will be released in 2016.

- Near infrared and visible.

  - CARMENES (Calar Alto high-Resolution search for M dwarfs with Exoearths with Near-infrared and optical Échelle Spectrographs, Quirrenbach et al. 2012) is a next-generation instrument being built for the 3.5 m telescope at the Calar Alto Observatory by a consortium of German and Spanish institutions. It consists of two separated spectrographs covering the wavelength ranges from 0.5 to 1.0 μm and from 1.0 to 1.7 μm with spectral resolutions R = 82,000, each of which shall perform high-accuracy radial-velocity measurements ($\sim$1 m/s) with long-term stability. The fundamental science objective of CARMENES is to carry out a survey of $\sim$300 M dwarfs with the goal of detecting low-mass planets in their habitable zones. The CARMENES first light is expected to occur before the end of 2015.

2 Analysis

2.1 Spectra compilation

We have mined the ESO public catalogues[VI] (advanced data products) for high-resolution spectra of M dwarfs that are potential targets for exoplanet hunting. In particular, we have downloaded all UVES spectra[VII] of M dwarfs in the preliminary list of targets of CARMENES, the German-Spanish optical-near infrared spectrograph for the 3.5 m Calar Alto telescope[VIII]. Besides, we have compiled the number of HARPS spectra[IX] for our sample of 2131 stars: see Table 5, Fig. 4 and, in the appendix, Table 10.

In resume, we have correlated CARMENCITA database stars with these catalogues. We have adopted CARMENCITA classification system based on priorities and divided into four classes (a detailed description is provided in the MSc thesis by González-Álvarez 2014):

- *Alpha*: maximum priority.
- *Beta*: second-priority stars.
- *Gamma*: backup weak stars.
- *Delta*: binary stars (companions located closer than 5 arcsec).

Table 5: Number of stars of our sample which spectra are present in HARPS and UVES databases.

Class	UVES	HARPS	Stars	UVES respect to total
Alpha	32	111	361	1.5%
Beta	4	23	198	0.2%
Gamma	11	61	1262	0.5%
Delta	14	41	272	0.7%
Total	61	236	2093	2.9%

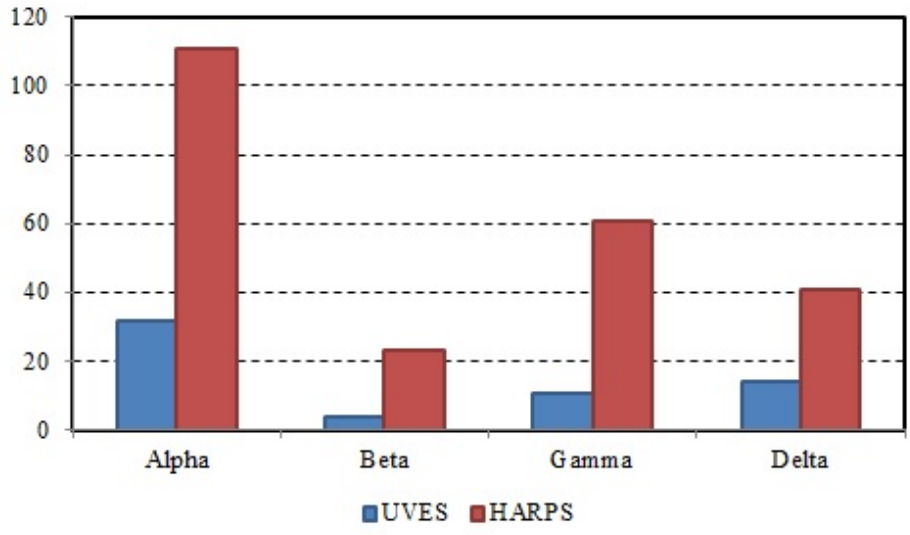

Figure 4: Number of stars of our sample which spectra are present in HARPS and UVES databases.

Let's explain this in more detail. Both HARPS and UVES query forms are identical. We must either introduce the coordinates of an object or its SIMBAD name:

[VI] http://archive.eso.org/eso/eso_archive_adp.html
[VII] http://archive.eso.org/wdb/wdb/adp/phase3_spectral/form
[VIII] http://carmenes.caha.es
[IX] http://archive.eso.org/wdb/wdb/eso/repro/form

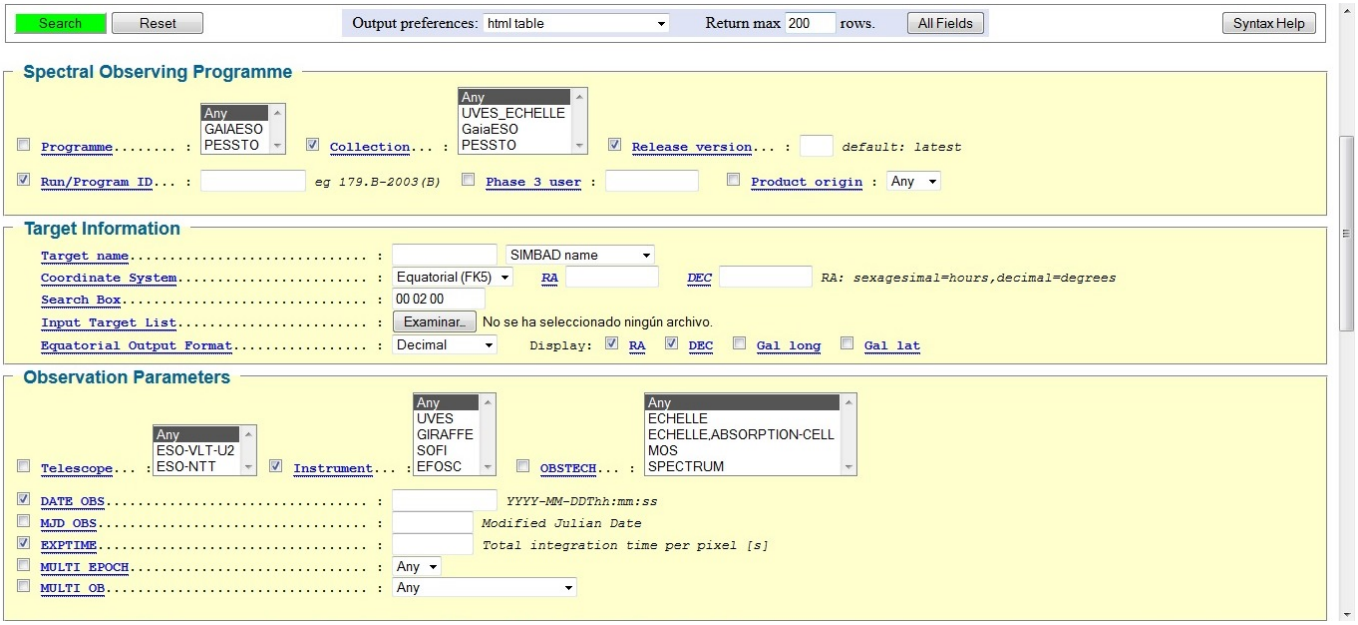

Figure 5: ESO advanced data products (UVES).

Then, the query form they retrieves a list of all the available spectra:

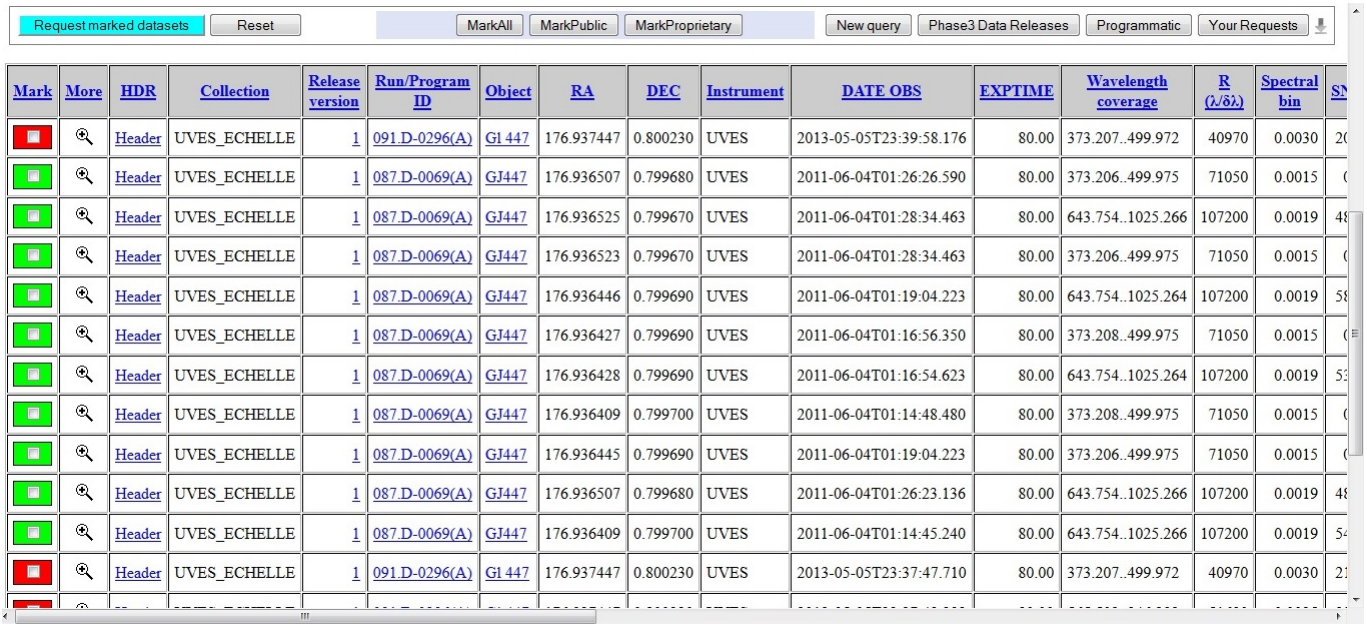

Mark	More	HDR	Collection	Release version	Run/Program ID	Object	RA	DEC	Instrument	DATE OBS	EXPTIME	Wavelength coverage	R (λ/δλ)	Spectral bin	SN
		Header	UVES_ECHELLE	1	091.D-0296(A)	GI 447	176.937447	0.800230	UVES	2013-05-05T23:39:58.176	80.00	373.207..499.972	40970	0.0030	20
		Header	UVES_ECHELLE	1	087.D-0069(A)	GJ447	176.936507	0.799680	UVES	2011-06-04T01:26:26.590	80.00	373.206..499.975	71050	0.0015	(
		Header	UVES_ECHELLE	1	087.D-0069(A)	GJ447	176.936525	0.799670	UVES	2011-06-04T01:28:34.463	80.00	643.754..1025.266	107200	0.0019	48
		Header	UVES_ECHELLE	1	087.D-0069(A)	GJ447	176.936523	0.799670	UVES	2011-06-04T01:28:34.463	80.00	373.206..499.975	71050	0.0015	(
		Header	UVES_ECHELLE	1	087.D-0069(A)	GJ447	176.936446	0.799690	UVES	2011-06-04T01:19:04.223	80.00	643.754..1025.264	107200	0.0019	58
		Header	UVES_ECHELLE	1	087.D-0069(A)	GJ447	176.936427	0.799690	UVES	2011-06-04T01:16:56.350	80.00	373.208..499.975	71050	0.0015	(
		Header	UVES_ECHELLE	1	087.D-0069(A)	GJ447	176.936428	0.799690	UVES	2011-06-04T01:16:54.623	80.00	643.754..1025.264	107200	0.0019	53
		Header	UVES_ECHELLE	1	087.D-0069(A)	GJ447	176.936409	0.799700	UVES	2011-06-04T01:14:48.480	80.00	373.208..499.975	71050	0.0015	(
		Header	UVES_ECHELLE	1	087.D-0069(A)	GJ447	176.936445	0.799690	UVES	2011-06-04T01:19:04.223	80.00	373.206..499.975	71050	0.0015	(
		Header	UVES_ECHELLE	1	087.D-0069(A)	GJ447	176.936507	0.799680	UVES	2011-06-04T01:26:23.136	80.00	643.754..1025.266	107200	0.0019	48
		Header	UVES_ECHELLE	1	087.D-0069(A)	GJ447	176.936409	0.799700	UVES	2011-06-04T01:14:45.240	80.00	643.754..1025.266	107200	0.0019	54
		Header	UVES_ECHELLE	1	091.D-0296(A)	GI 447	176.937447	0.800230	UVES	2013-05-05T23:37:47.710	80.00	373.207..499.972	40970	0.0030	21

Figure 6: Example of UVES query (FI Vir).

Why have we chosen to show this concrete query? Because not all the data are currently available: during the first year, only the researcher who obtained them is able to use them (shown in red). After this period, every investigator may download the spectra (shown in green). This can be seen in the appendix (Table 10, unavailable spectra due to the one-year ownership period).

Going on with this example, we see that there is a wide information as exposure time, UVES channel and signal-to-noise ratio. After having logged in the ESO User Portal and submitting our request, we receive a confirmation email and then are able to download the *.fits* spectra, as well as a *.txt* README archive:

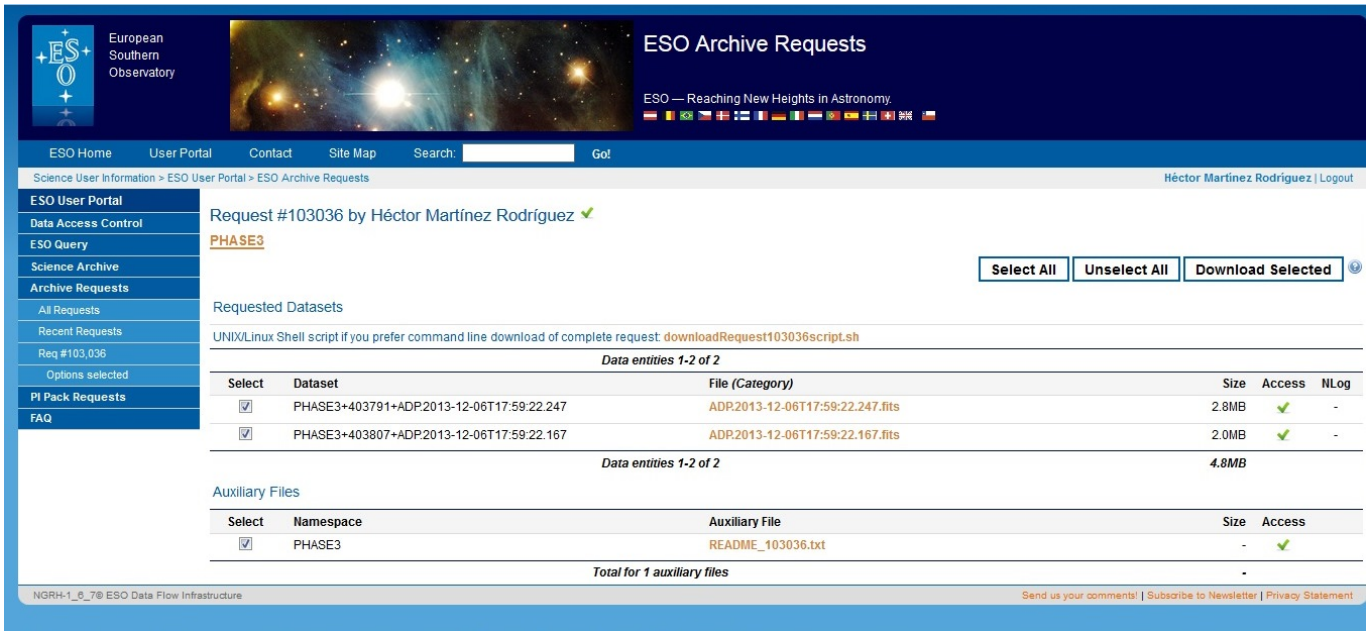

Figure 7: Example of UVES data request (FI Vir).

Clearly, there must be a more efficient and fast search method instead of introducing stars one by one. HARPS and UVES query forms allow to introduce a list of targets. Thanks to the software Topcat, where we had a table with all the data of our sample, we separated the stars in four ASCII tables according to their class (Alpha, Beta, Gamma and Delta) and then saved their coordinates RA J2000 and DEC J2000. This is the reason why we will see in the appendix tables a clear distinction based on these four classes. Moreover, all our calculations are based on this sorting.

In section 1.2.2 we saw UVES arms. As the accessible wavelength ranges are broad, it is logical to suppose that every arm may have several channels. When looking for spectra in UVES catalogue, we have found a total of 12 channels, as shown in the appendix (Table 11). We must remark that not all our spectra have proven to be useful because of several reasons:

- Low S/N ratio.
- Cosmic rays. We have not cleaned them. Sometimes, they impeded us to see emission or absorption lines.
- Bad quality. Some spectra presented unreal shapes, above all next to the edge in the blue arms and next to Hα line in the red arms.
- Primary companions. In few cases, due to the query procedure (search box with a default value set to 2 arcmin), the retrieved spectra belonged to the primary and hotter companions of our M stars. Note that Delta, and even some Gamma stars, are binary systems (see also Table 10).

These situations are shown in Table 11, too. We conclude that, regarding the 61 stars (32+4+11+14) of our sample present in UVES database, we have downloaded a total of 128 spectra (72+7+14+35), from which 37 should be thrown away (some stars have spectra in more than one channel). We must mention that UVES spectra cannot be seen with the environment IRAF in a straightforward way: some problems with their headers (one-dimension spectra) require them to be converted with IDL. Professor David Montes kindly performed this single task.

We have measured pseudo-equivalent widths of lines in absorption and emission and rotational velocities on these high-resolution UVES spectra. We will do a separate description of our methods in subsections 2.3 and 2.5.

2.2 Spectra

Obviously, we found more than one spectrum for almost every one of our stars. When manipulating all our spectra with IDL (professor David Montes), this program returned ASCII files of them. First of all, here we show the spectra of the stars for which we had three or more spectral ranges.

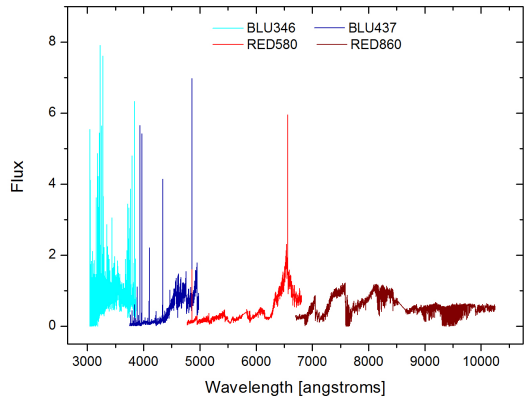

(a) J01390–179 spectra.

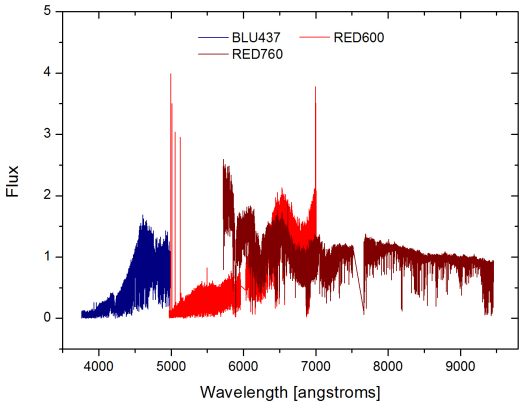

(b) J04376–110 spectra.

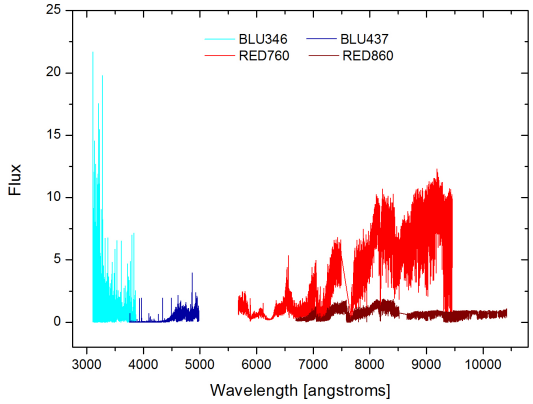

(c) J10482–113 spectra.

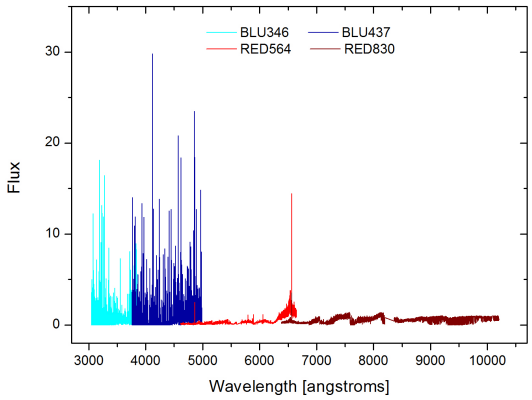

(d) J10564+070 spectra.

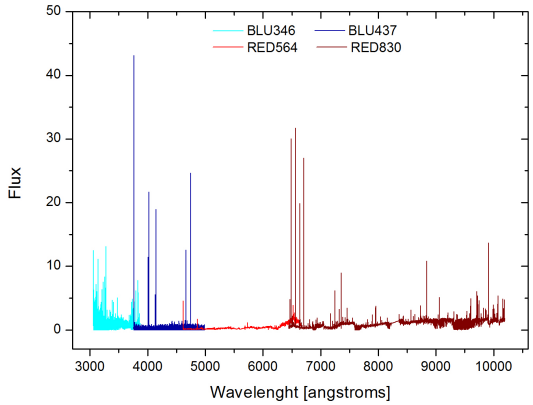

(e) J12189+111 spectra.

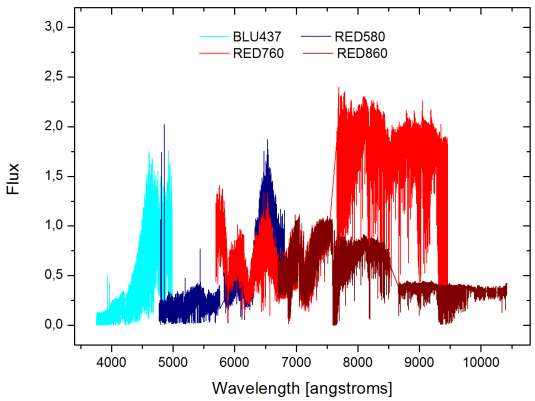

(f) J22532–142 spectra.

Figure 8: Spectra of the stars for which we had three or more spectral ranges.

We have conveniently normalized them taking different wavelengths as a reference:

Table 6: Reference wavelength for every channel.

Channel	BLU346	BLU390	BLU437	RED564	RED580	RED760	RED830	RED860
λ_{ref}(Å)	3550	4400	4600	6400	6400	7400	7400	7400

On the other hand, it is very interesting to compare stars of different spectral type when considering the same channel. Applying these last normalizations (Table 6), we show in Figs. 9 and 10 most of our channels and mention their most outstanding spectral features.

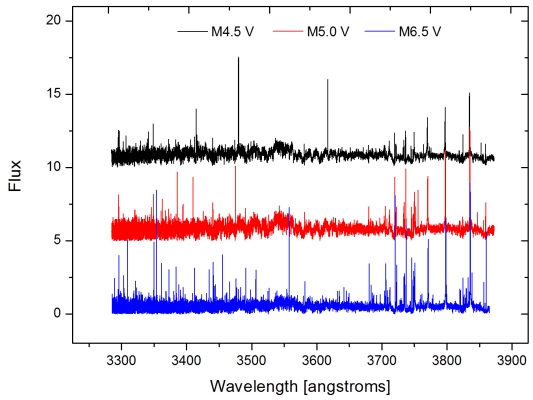

(a) BLU346 channel. Balmer series.

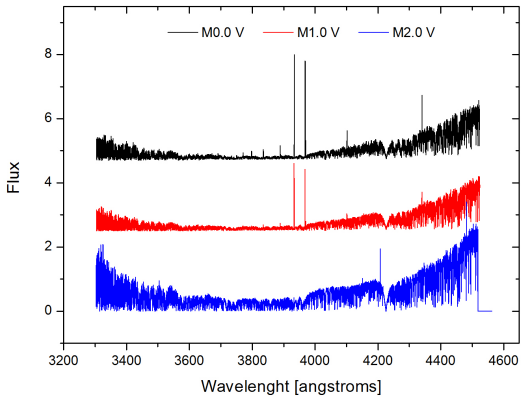

(b) BLU390 channel. Ca II H & K, Hδ, Hγ.

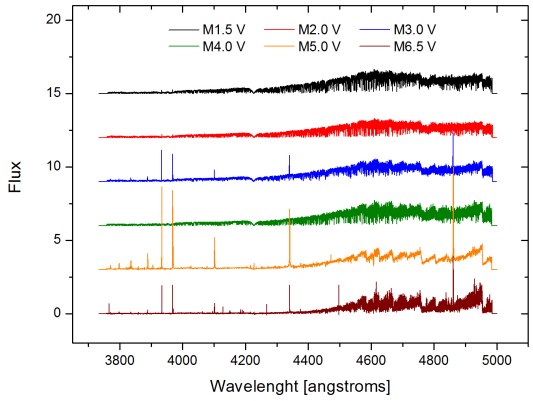

(c) BLU437 channel. Ca II H & K, Hδ, Hγ, Hβ.

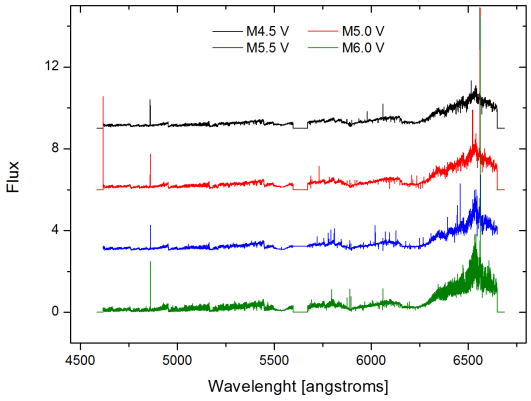

(d) RED564 channel. Hβ, Hα.

Figure 9: Spectra compared in most of the available arms. The stars have been ordered from earliest type to latest type from top to bottom.

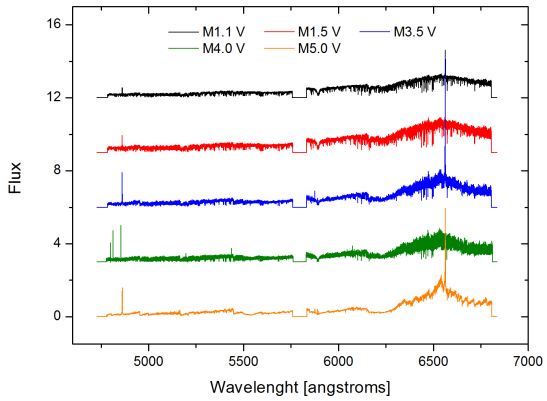

(a) RED580 channel. Hβ, Hα.

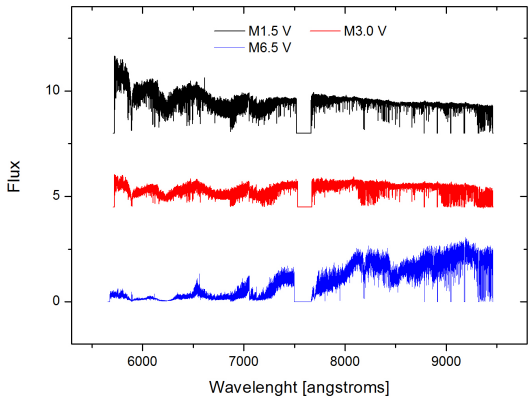

(b) RED760 channel. Hα, molecular bands.

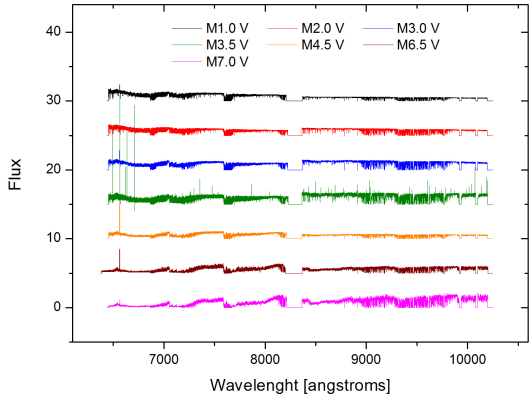

(c) RED830 channel. Hα, molecular bands.

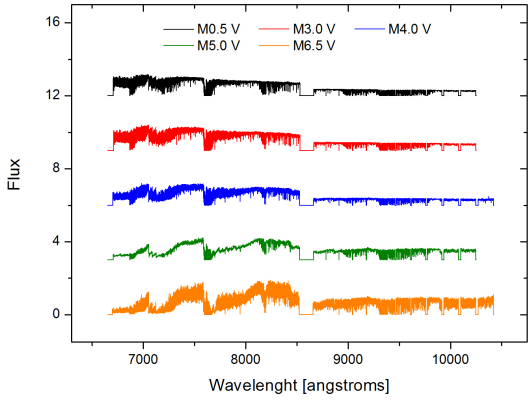

(d) RED860 channel. Molecular bands.

Figure 10: Spectra compared in most of the available arms. The stars have been ordered from earliest type to latest type from top to bottom (cont.).

2.3 Pseudo-equivalent widths

Let's now talk about *pEW*s. We have studied our downloaded *.fits* spectra (transformed to readable IRAF format) thanks to the software IRAF: the `splot` command opens an emergent window where the input spectrum is shown. IRAF automatically assigns positive *pEW* values for emission lines and negative values for absorption lines. There are two instructions with which we could measure *pEW*s by selecting two points: `k`, which performs a gaussian fitting, and `e`, which performs an integration. Of course, it is necessary to enlarge the spectrum close to the desired line (`w`+`e`, then `e`), as shown in Fig. 11. We can return to the original view with `w`+`a` or directly clean the `splot` window with `c` or `r`.

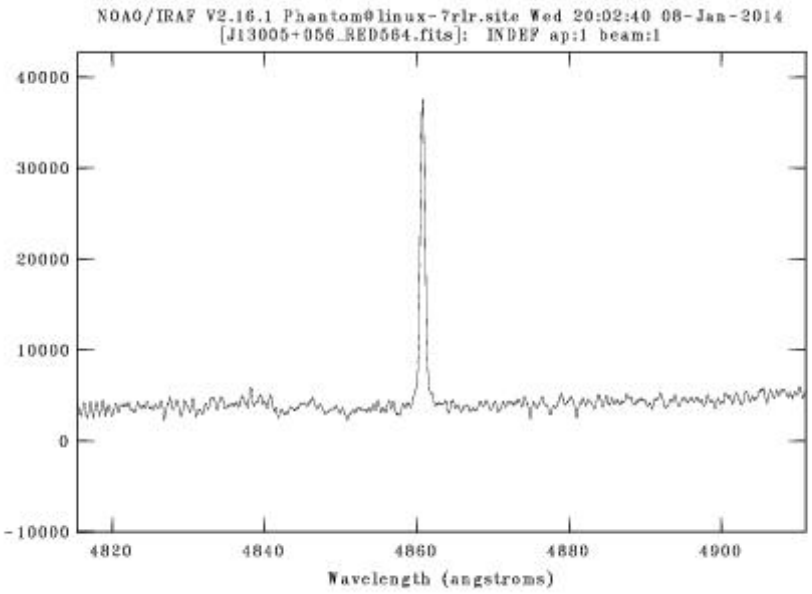

Figure 11: J13005+056 $H\beta$ emission.

The vertical axis of the spectrum is not normalized to unity. This is why we measure pEWs: there is no way we can know the exact continuum radiation position. We have taken three pEWs per line and have obtained the final result as the arithmetic mean of them with their standard deviation as the statistical error. Regarding the used command, taking into account this trouble related with the pseudocontinuum, we have chosen to integrate (`e`).

Theoretically, we could enlarge the image to make our measurements, but it would be an unreal result because of what we have just said about the continuum position. Besides, the statistical error would just be negligible and, again, an unacceptable result. Not to underestimate the continuum, we have taken "rude" measurements by making small vertical movements along the lines centres:

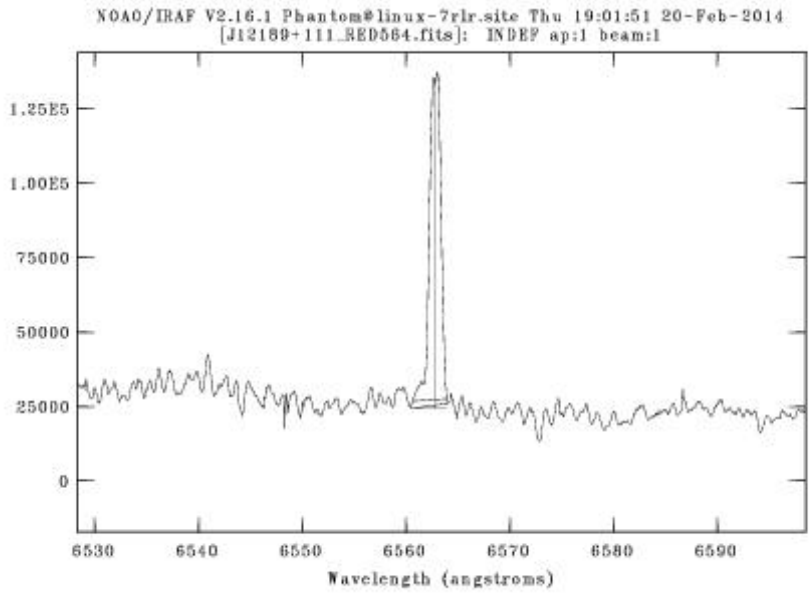

Figure 12: Measurement of J12189+111 $H\alpha$ emission line pEW (command `e`).

2.4 $H\alpha$ line measurements

We are specially interested in Hα pEWs, as in CARMENCITA database there are previous measurements with which we can compare our results. Furthermore, these pEWs will help us to find low-activity stars. We have measured 37 pEWs for 35 stars (Hα line appeared in two different channels for two of these stars). See Fig. 13a.

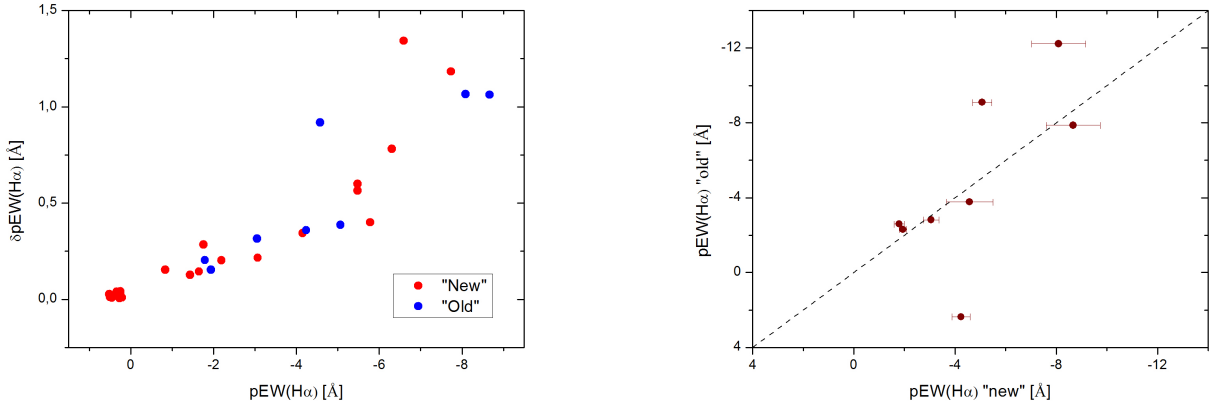

(a) δpEW(Hα) vs pEW(Hα).

(b) pEW(Hα) "old" vs pEW(Hα) "new".

Figure 13: Hα line measurements. *Left panel*: pEWs of Hα line pEW(Hα) and their errors δpEW(Hα). *Right panel*: pEWs of Hα line, eight of which were already present in CARMENCITA. We have called these stars "old", while the other ones have been denoted by "new", notation that we will employ successively.

Thus, in Fig. 13b we have compared our eight values with the ones belonging to CARMENCITA. There are three stars that do not fall in the line of equality, as can be seen in Table 7 :

Table 7: Hα line measurements.

Karmn	Hα "new"	Hα "old"
J05068–215E	-1.94 ± 0.15	–2.31
J08536–034[a]	-8.1 ± 1.1	–12.2
J10482–113	-3.1 ± 0.3	–2.8
J10564+070	-8.7 ± 1.1	–7.9
J16555–083[a]	-4.2 ± 0.4	+2.4
J02164+135	-4.6 ± 0.9	–3.8
J01390–179[a]	-5.1 ± 0.4	–9.1
J04376–024	-1.8 ± 0.2	–2.6

[a] Striking points.

We are convinced that the discrepancy concerning J16555–083 is due to a typing mistake, as absorptions and emissions are perfectly distinguishable when studying a spectrum, while we find no explanation for the other two cases. We think it could be due to variability (given the different epoch of the observations). We will study the possible relationship between activity and spectral type in subsection 3.2.

2.5 Rotational velocities

Let's focus on rotational velocities. As we saw in subsection 1.1.2, the rotation of an M dwarf is closely related to its chromospheric activity: the more active the star is, the faster it will rotate. Typically, M dwarfs rotational velocities are located in the range 2 – 30 km/s, which can be seen in Reiners et al. (2012) and in CARMENCITA database[X]. To be precise, our aim is to calculate rotational velocities with our UVES spectra and compare the results with the ones shown in CARMENCITA if possible.

We have done cross-correlation profiles (see Tonry & Davis 1979; Basri et al. 2000; Reiners et al. 2012) with IRAF thanks to the task `fxcor`. It needs a "template" star with which to compare the problem star, i.e., the relative broadening of the spectral lines one by one; thus, template stars are the most important part of this calculation. To find low-rotation stars in our sample, we have have taken the ones with Hα absorptions, that is to say, the less active stars (see Fig. 25a in the appendix).

Obviously, these correlation profiles must be done in the same wavelength range, reason why we separated all our spectra depending on their channel in different directories. We have restricted ourselves to BLU437, RED564 and RED580 channels, as in shorter wavelengths there are barely spectral lines and further away from Hα molecular bands (TiO) appear and would spoil the correlation. On the other hand, we found that some spectra were not adequate when correlating them with another ones, so not all our low-activity stars have been chosen as templates. These stars have been the selected ones[XI]:

- J02442+255 (M3.0).
- J17052–050 (M2.0).
- J22532–142 (M4.0).
- J22559+057 (M1.0).
- J10289+008 (M2.0).
- J22021+014 (M0.5).
- J20574+223 (M2.0).

We have correlated all the templates with all the stars, including templates themselves to find if they are low-rotation stars and, hence, adequate. However, as correlating an M1 star with an M9 star, for instance, would not have physical sense (remember Figs. 9 and 10), the results must be carefully and conveniently analysed. We have not had this problem when measuring $vsini$ for the reference stars, as their spectral types are quite similar.

IRAF returns the FWHM resulting from the correlation between the template and the problem star, so we need a way to "convert" FWHMs into rotational velocities ($v \sin i$). Our analysis makes use of the program `starmod` developed at Penn State University (Huenemoerder & Barden 1984; Barden 1985) and modified more recently by the UCM stellar group (Montes et al. 2000). This program is used to apply the spectral subtraction technique (see Montes et al. 1995) and can be employed to construct an artificially rotationally broadened spectrum with the desired value of $v \sin i$. Correlating the original spectrum with the broadened one, we can build an interpolating function that relates FWHMs and rotational velocities. As `starmod` needs a pixel interval that, according to our trials, cannot surpass 4000 pixels, we have followed a long process to aim our goal:

1. When we were studying the stars that could be used as templates, we found the most appropriate wavelength range for every template where to perform the correlation.
2. Employing the task `scopy`, we cut the spectra in the desired wavelength range.

[X] http://carmenes.caha.es/ext/armada/

[XI] From now on, for simplicity, we omit that all our stars belong to the main sequence. We denote by 0.0, 0.5, 1.0 and so on spectral types M0.0, M0.5 and M1.0, while M10.0 means L0.0 spectral type (SpT).

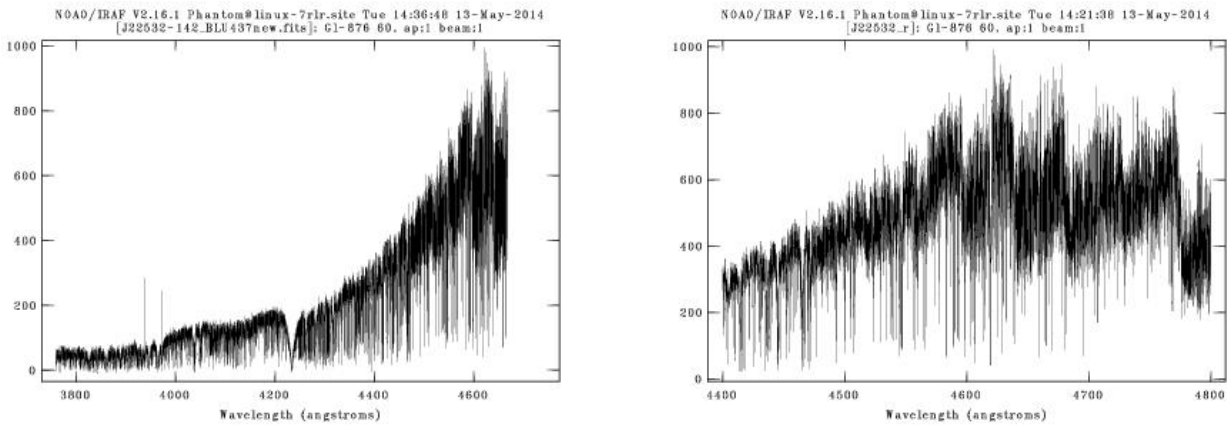

Figure 14: *Left panel*: J22532–142 complete spectrum in the BLU437 channel. *Right panel*: J22532–142 spectrum in the wavelength range 4400-4800 $\mathring{A}$.

3. In this last spectra, typing `$`, we passed from wavelengths to pixels.

4. As we found that we were always dealing with 10^4 pixels, we had to rebin all our cut spectra to have at most 4000. The IRAF task `dispcor`, using a parameter that is called `dw`, enables to fix the wavelength interval per pixel and, consequently, the total number of pixels. It implies, of course, a certain loss of resolution.

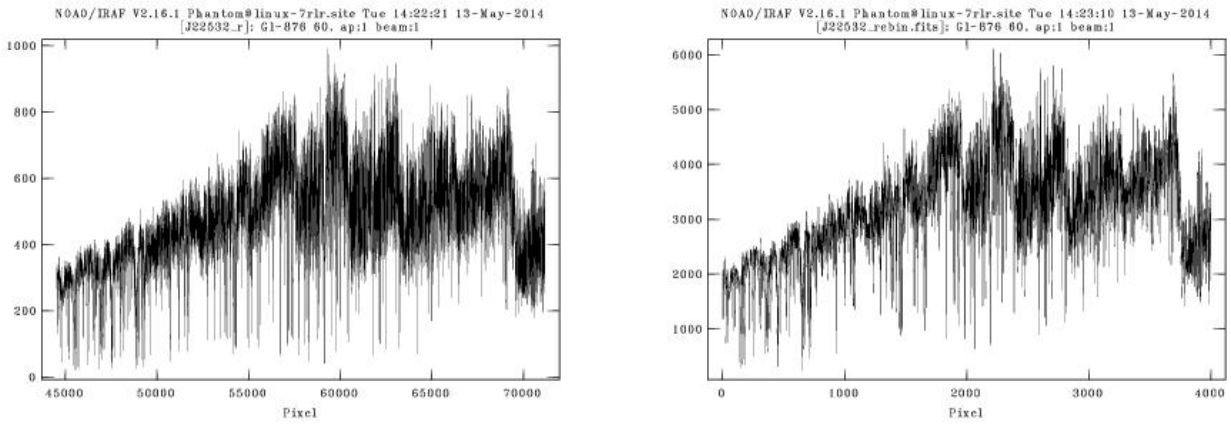

Figure 15: *Left panel*: J22532–142 cut spectrum in a huge pixel range. *Right panel*: J22532–142 cut and rebinned spectrum in the pixel range 0 - 4000.

5. After all these steps, we were finally able to perform broadenings with `starmod`. We did it for several values of $v \sin i$ [km/s]: 1, 2, 3, 4, 5, 7, 8, 9, 10, 12, 14, 15, 17, 20, 25 and 30.

```
###### A '#' begins a comment till the end of the line
###### The syntax is 'KEYWORD = value' with one statement per line

###### GENERAL INFORMATION
IM_PATH  =                      # path of fits spectra (optional)
OBJ_NAME = J22532_rebin.fits    # object name

###### OUTPUT SPECTRA
SYN_SPEC = YES                 # write output spectra: YES/NO
   SYN_NAME = J22532_rot30.fits  # synthetised spectrum name
   SUB_NAME = sub.fits              # substracted spectrum name (if SYN_SPEC =YES)


###### INTERPOLATION PARAMETERS
N_ITER =  4                    # iteration number: integer
PIX_ZONE = 1 1000               # pixel range for the fit: 2 integers
PIX_EXCL =                      # skip pixel subrange: 2 integers (optional)
PIX_EXCL =                      # skip pixel subrange: 2 integers (optional)
PIX_EXCL =                      # skip pixel subrange: 2 integers (optional)
PIX_EXCL =                      # skip pixel subrange: 2 integers (optional)
PIX_EXCL =                      # skip pixel subrange: 2 integers (optional)


###### PRIMARY STAR
PRM_NAME = J22532_rebin.fits   # primary name
PRM_RAD  = 0 fix                # doppler shift: float, keyword (var/fix)
PRM_ROT  = 30 fix               # doppler broadening: float, keyword (var/fix)
PRM_WGT  = 1 fix                # weight: float, keyword (var/fix)


###### SECONDARY STAR
SEC_NAME =  NONE                # secondary name: name/NONE
   SEC_RAD  =                   # doppler shift: float;
   SEC_ROT  =                   # doppler broadening: float;
   SEC_WGT  =                   # weight: float, keyword (var/fix)

###### TERTIARY STAR
TER_NAME =  NONE                # tertiary name: name/NONE
   TER_RAD  =                   # doppler shift: float, keyword (var/fix)
   TER_ROT  =                   # doppler broadening: float, keyword (var/fix)
   TER_WGT  =                   # weight: float, keyword (var/fix)

###### SPECTRA FOPRMAT
   MODE=  mult                  # spectra format if multidimensionnal: mult/ech
   APERTURE = 1                 # aperture number : integer
   BAND=                        # band number : integer (optional)

################################## FIN ######################################
```

Figure 16: Example of `starmod` screen for J22532–142 and a broadening of 30 km/s.

6. Using `fxcor`, we correlated every cut and rebinned spectrum with itself broadened at all the mentioned values, found the FWHMs (see Fig. 17) and recorded them to build calibration curves for all the templates, as shown in Figs. 18 and 27 (the last one in the appendix). Then, we built interpolating functions for all the templates.

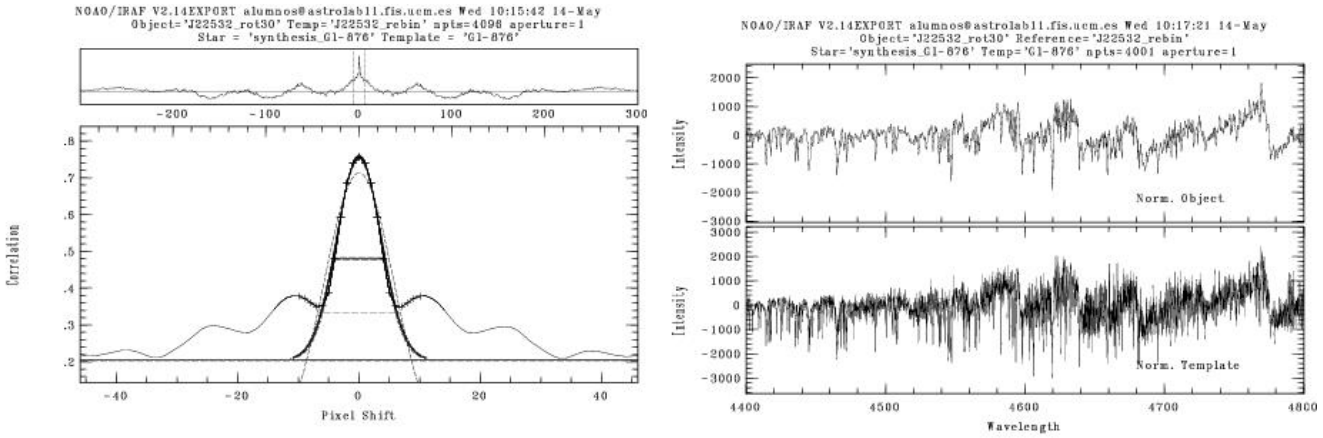

Figure 17: J22532–142 rebinned and cut spectrum correlated with itself broadened at 30 km/s. Broadening can perfectly be seen in the right panel.

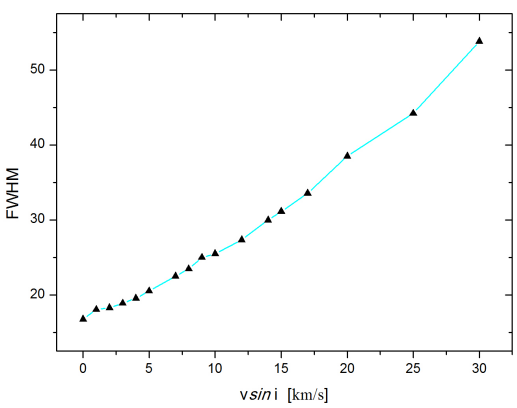

(a) J22532–142 (BLU437 channel).

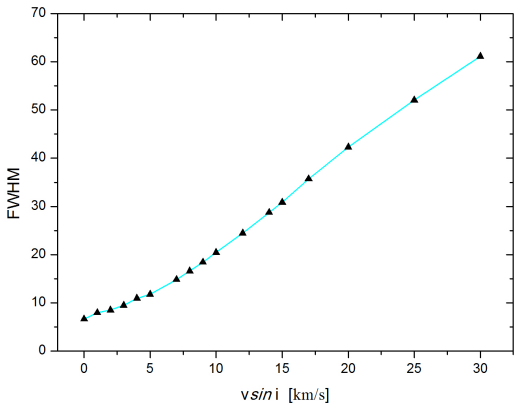

(b) J22532–142 (RED580 channel).

Figure 18: Calibration curves for the template star J22532–142 in two different channels. Their shape is practically identical but their upper and lower FWHMs are quite different, which implies that the curve in the right panel has a bigger FWHM range.

7. Finally, we correlated all our downloaded spectra with the templates. After measuring the FWHMs, we invoked our interpolating functions and found the values of $v \sin i$ for every star. Errors have been obtained thanks to TDR parameter (Tonry & Davis 1979), returned by `fxcor` in a *.log* file:

$$\Delta\, v \sin i \;=\; \frac{v \sin i}{1 + \mathrm{TDR}}$$

3 Results and discussion

3.1 *pEW*s vs *pEW*($H\alpha$)

We want to compare all the lines with Hα and to study the relationship between pEWs and spectral types. All the measurements are shown in the appendix (Tables 12 and 13), as well as the graphics of the pEWs compared to Hα pEW (Figs. 23 and 24):

In this subsection, we have done linear fits for all the pEWs pairs of data: we are interested in finding if there is any relationship between Hα and the other spectral lines. We show all the R^2 coefficients in Table 8:

Table 8: Pearson coefficients for the linear fits of the previous graphics, Figs. 23 and 24 in the appendix.

Line	Hη	Hζ	Ca II K	Ca II H	Hϵ	Hδ	Hγ	Hβ	He I D_3	Na I D_2	Na I D_1
R^2	0.4444	0.8741	0.2984	0.2787	0.0688	0.11810	0.4492	0.5463	0.2327	0.3359	0.2809

We extract several conclusions:

- The only fit that approaches to a straight line corresponds to Hζ line ($R^2 = 0.8741$). This is why we are showing it in Fig. 19.

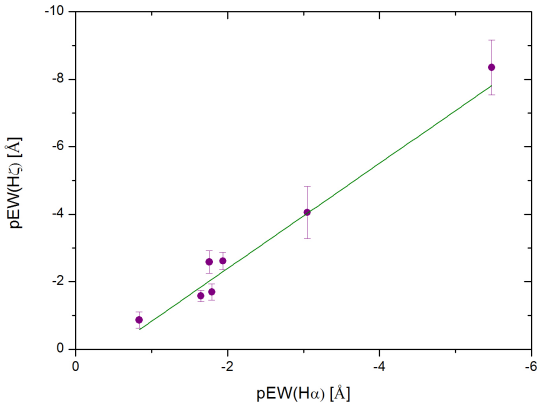

Figure 19: Linear fit for pEW(Hζ) vs pEW(Hα). The number of points is certainly limited, but the resulting linear fit is fine.

- Pearson coefficients for sodium, helium and calcium fits are very low. Although there exists a tendency, some stars have high pEWs and worsen the linear fits.
- Taking a look at Hγ, Hδ and Hϵ graphics we see that, in all the cases, there are two stars that get out of our linear fit:
  - J10482–113 (SpT 6.5).
  - J05068–215W (SpT 3.5).

  Which is probably caused by flares, as these phenomena alter Balmer series coefficients.
- The same situation occurs when we view sodium doublet graphics, specially D2 line. Three stars have a pEW (Na I D2) much bigger than their pEW(Hα):
  - J08298+267 (SpT 6.5).
  - Again, J10482–113.
  - J16555–083 (SpT 6.5).

In this case, apart from the strong sodium peaks caused by flares, there is a simple explanation: when approaching Hα line, molecular bands begin to appear and the spectrum ascends when compared to sodium doublet region (pseudo-continuum). If we normalized the spectrum, pEW(Hα) would be bigger than the sodium ones, as expected.

- Hβ fitting is not very good.

3.2 *pEW*s vs spectrals types

Graphical relationships between pEWs and spectral types are displayed in Figs. 25 and 26 in the appendix. Let's take a deep look at Fig. 25a. Most of our stars have a low activity. Fifteen of them present weak absorptions ($pEW > 0$). Their spectral types are 4.0 (J14342–125, J22532–142), 3.5 (J16554–083N), 3.0 (J02442+255, J06548+332), 2.0 (J10289+008, J17052–050, J20574+223), 1.5 (J04376–110, J13457+148, J22565+165), 1.0 (J15598–082, J22559+057) and 0.5 (J06105–218, J22021+014), so all of them are early-type stars.

On the other hand, the most active ones are late-type stars (SpT $\geq$ 4.0). Three of them are really outstanding: J08536–034 (9.0), J23064–050 (8.0) and J10564+070 (6.5), the biggest Hα peak.

Regarding the sodium doublet, we are only interested in emission peaks, i.e., we have not measured absorptions. We clearly see in the similar Figs. 25b and 25c that, the later the spectral types are, the bigger their emissions peaks are. The weakest peak corresponds to J05068–215E (1.5), while the strongest ones belong to J08536–034 (see the big uncertainty), J10482–113 and J16555–083.

He I D3 line is lightly different (Fig. 25d). In general, all the emission pEWs are very weak. Late-type stars have both strong and weak peaks. The biggest pEWs correspond to J10564+070 (6.5) and J01390–179 (5.0), and the weakest one, to J04595+017 (0.0). These Na I and He I lines are observed as emission peaks when the stars present flares, which happens, as we already know, in high-activity stars (that are, in general, the ones with latest type).

Let's deal now with Balmer lines. Our biggest pEWs are associated with Hβ line. The least ones belong to early-type stars (0.0, 1.0, 3.0, 3.5 and, only in one case, 6.0). We have much more Hβ measurements than in the cases of Hγ, Hδ, Hϵ, Hζ and Hη. Generally, as it happened with sodium, weak peaks are associated with early-type stars and strong emissions with late-type stars. Note that there are not absorptions.

- Hβ (Fig. 25e). There are two really high pEWs (J04403-055, 6.0, the strongest emission peak, and J10564+070, 6.5) and several weak peaks: J04595+017 (0.0), J07403–174 (6.0), J04376–024 (1.1), J14544+161 (1.0), J16554–083N (3.5) and J18554+084 (3.0).

- Hγ (Fig. 25f). Again, there are two strong peaks: J10564+070 and J01390–179 (5.0). Some of the lowest pEWs correspond to the stars recently mentioned for the case of Hβ: J04595+017, J18451+063 (1.0), J04376–024, J14544+161 and J18554+084 (3.0).

- Hδ (Fig. 26a). Except in the cases of J01390–179 (the strongest peak), J10564+070, J10482–113 and J05068–215W (3.5), all the emission peaks are very weak.

- Hϵ (Fig. 26b). The four high pEWs correspond to exactly the same stars we have just mentioned.

- Hζ (Fig. 26e). There is only one strong emission peak: J05068–215W.

- Hη (Fig. 26f). There is not a clear relationship between pEW and spectral type. All the peaks are very weak. Again, the strongest one corresponds to J05068–215W.

Finally, Ca II H & K lines (Figs. 26c and 26d) deserve a special mention. They present the highest pEWs of all our lines, including Hα. Similarly to the sodium doublet, as we expected, the two graphics are analogous. Except in the case of the weak emission of J04352–161 (7.0), all the strong peaks are associated with late-type stars: the highest emission for both lines belongs to J01390–179. The other two peaks are the stars J10564+070 and J10482–113.

The three of them have constantly appeared throughout this section when mentioning high pEWs. Hence, we can surely assert that their spectra present flares, which explain these obtained pseudo-equivalent widths. They are also the reason for all the other strong peaks, above all sodium and helium lines: we will study them in subsection 3.3.

3.3 Flares

As we already know, high pEWs (strong emission peaks) likely indicate the existence of flares. From the results derived in subsections 3.1 and 3.2, we have the following stars:

- J08298+267
- J10482–113
- J16555–083
- J01390–179
- J08536–034
- J10564+070
- J04403–055
- J05068–215W

There is a very reliable way to determine whether emission lines are caused by flares or whether they have their origin in other physical phenomena: Balmer decrement $pEW(\mathrm{H}\alpha)/\mathrm{pEW}(\mathrm{H}\beta)$. This quotient should be relatively low in the case of flares (Hawley & Pettersen 1991; Montes et al. 1999). We show it in Fig. 20:

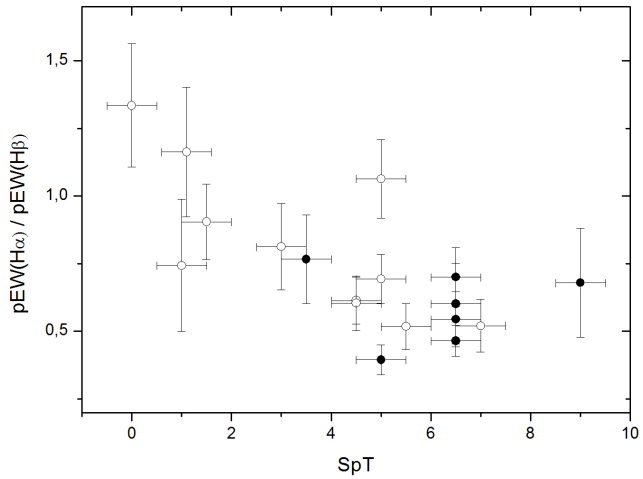

Figure 20: Balmer decrement vs spectral type. Stars that likely present flares are depicted as filled circles. We had no $pEW(\mathrm{H}\alpha)$ value for J04403–055.

Indeed, this Balmer decrement is low in the case of flares when compared to the other stars. There is a spectral line related with this phenomena we briefly mentioned in subsection 1.1.2: Ca I wide absorption at 4226 Å. Stars that present flares have a strong emission peak overlapping this absorption. From these eight stars, we only had BLU437 channel spectra for four of them:

Table 9: pEW of Ca I λ4226 Å line.

Karmn	pEW [Å]
J10482–113	-2.42 ± 0.50
J10564+070	-10.4 ± 1.2
J04403–055	...
J01390–179	-6.09 ± 0.58

3.4 Obtained values of $v \sin i$

We have measured $v \sin i$ for 24 stars, from which 17 have a registered value in CARMENCITA database. The results are displayed in Table 14 in the appendix. We point out that we have had several problems to select a wavelength where to calculate the FWHM. Regarding the final results, we must do two remarks:

- Narrow profiles. For eight stars, including all our templates, we have obtained FWHM values smaller than

the ones corresponding $v \sin i = 0^*$ in the calibration curves (Figs. 18 and 27). When comparing them to CARMENCITA values (2.5 km/s, detection limit estimated by Browning et al. 2010), we think the upper limit must be close to 2−3 km/s. We are unable to obtain the exact values of these rotational velocities, which are not null.

- In general, our results differ very little from the ones of CARMENCITA (see Fig. 21). There are few exceptions. The most remarkable ones are J22021+014 (White et al. 2007), J04376–024 and J18554+084. The first star is one of our templates. Correlating it with other three templates we have obtained a narrow profile, while CARMENCITA value is $v \sin i = 20.21 \pm 4.94$ km/s. There is no way we can explain this discrepancy. We think CARMENCITA value is wrong because of the stellar activity-rotation relationships which appear in the MSc thesis by González-Álvarez (2014).

In conclusion, we have found rotational velocities that, in general, agree with the previous values shown in CARMENCITA. This fact will allow CARMENES to discard stars with high $v \sin i$ values, as their radial velocity profiles would lack precision.

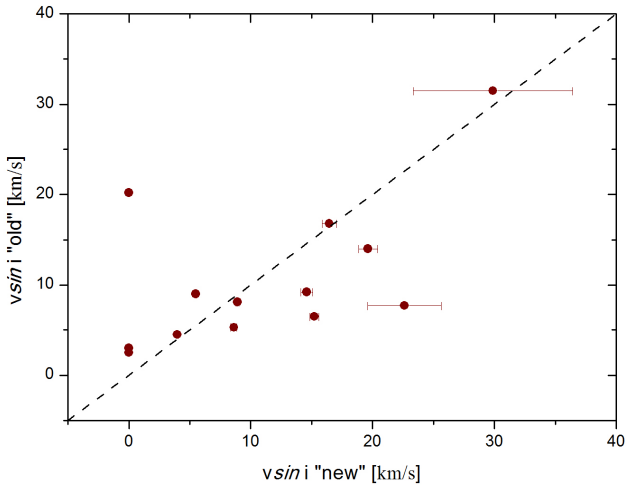

Figure 21: $v \sin i$ "old" vs $v \sin i$ "new". Most of our stars fall near the line of equality. The star J22021+014 is the point in the upper left side.

3.5 *pEW*s(Hα) vs rotational velocities

Finally, we have joined our results concerning $pEW(\mathrm{H}\alpha)$ and $v \sin i$ to find out if they are linked. In principle, we already know that our template stars have $v \sin i = 0^*$ and, on the other hand, we must be very careful with our stars that likely present flares studied in subsection 3.3. The results can be seen in Fig. 22.

Obviating our templates, we could have expected an approximate linear relationship between the two magnitudes that we do not see. There are two reasons that explain this fact:

- Stars with flares have high $pEW(\mathrm{H}\alpha)$ values that are not related to their rotational velocities.
- We have a high dispersion due to the inclination ($\sin i$). There is no way we can know the exact value of v unless we have photometric periods, which can indeed be seen in the MSc thesis by Hidalgo (2014). Hence, we have been unable to extract a reliable conclusion regarding the possible relation between pEWs(Hα) and rotational velocities.

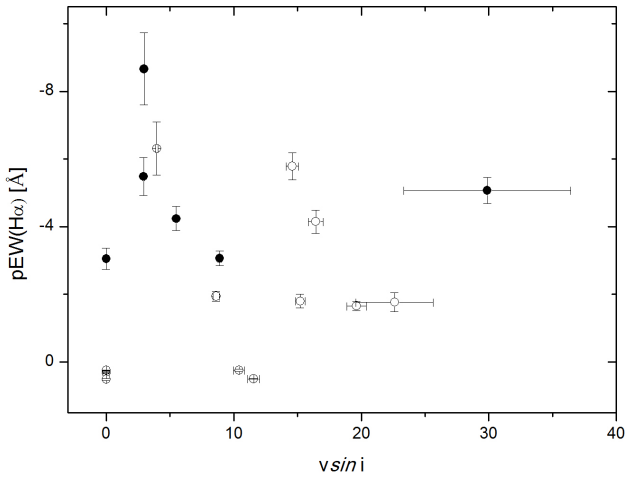

Figure 22: $pEW(\mathrm{H}\alpha)$ vs $v \sin i$. Again, stars that likely present flares are depicted as filled circles.

4 Conclusions and future research

We have mined the ESO public catalogue to find out how many stars of our sample of 2093 stars (CARMENCITA, February 2014) present spectra in HARPS and UVES databases. After having correlated these databases with CARMENCITA, as 236 stars appeared in HARPS catalogue and 61 in the one of UVES we have only downloaded UVES spectra. HARPS spectra were too numerous for us to study them. Our downloaded UVES spectra comprise a total of 128.

We have calculated the pEWs of Ca II H & K lines, He I D_3 line, Na I doublet D_1 & D_2 lines and Balmer series lines Hα, Hβ, Hγ, Hδ, Hη and Hζ. We have measured $pEW(\mathrm{H}\alpha)$ for 35 stars with a total of 27 new values, which has permitted us to identify the least active stars in our sample. On the other hand, we have found high-activity stars that probably present flares. We have studied the relation among the pEWs of all the lines and $pEW(\mathrm{H}\alpha)$ and have found no good correlations between them. As expected, after analysing the relationship between pEWs and spectral types we have concluded that late M dwarfs are usually more active than the early ones (results that broadly coincide with the ones of Robertson et al. 2013).

Then, we have focused on rotational velocities. Choosing our low-activity stars as "templates" of narrow lines, we have performed cross-correlation profiles in order to find $v \sin i$ for 24 stars, from which seven measurements are completely new. Narrow profiles, present for eight stars, are interesting because low rotational velocity values imply that radial velocity measurements performed by CARMENES will have a extremely high precision, of about 1 m/s. We have not found a relationship between $pEW(\mathrm{H}\alpha)$ and $v \sin i$. Regarding our excellent spectra concerning calibrations and cross-correlation profiles, we think we have improved the existing $v \sin i$ value for, at least, three stars (see section 3.4).

To sum up, our spectral characterisation will be helpful for CARMENES in order to choose observation targets from the input catalogue. Very precise radial velocities are an essential method to find stars that host exoplanets, which is the goal of this project. We expect our study of UVES spectra to be a reference for future analysis involving the numerous HARPS spectra of CARMENCITA database stars. Furthermore, we hope the exact values of the rotational velocities for our narrow profiles ($v \sin i = 0^*$) will be precisely measured.

Part of our analysis has appeared in a poster in an international scientific congress, "Cool Stars 18", The 18th Cool Stars, Stellar Systems and the Sun workshop (Montes et al. 2014). See the last page of the appendix.

References

Barden, S. C. 1985, ApJ, 295, 162

Basri, G. et al. 2000, ApJ, 538, 363

Browning, M. K. et al. 2010, AJ, 139, 504

Dekker, H. et al. 2000, SPIE, 4008, 534

Delfosse, X. et al. 1998, A&A, 331, 581

Demory, B. -O. et al. 2009, A&A, 505, 205-215

González-Álvarez, E. 2014, MSc thesis, Universidad Complutense de Madrid, Spain

Hall, J. C. 2008, Living Rev. Solar Phys., 5, 2

Hawley S. L., Pettersen B. R., 1991, ApJ, 378, 725

Hawley, S. L. et al. 1996, AJ, 112, 2799

Hidalgo, D. 2014, MSc thesis, Universidad Complutense de Madrid, Spain

Houdebine, E. R. 2010, MNRAS, 407, 1657

Huenemoerder, D. P., & Barden, S. C. 1984, BAAS, 16, 510

Jenkins, J. S. et al. 2009, ApJ, 704, 975

Marcy, G. W., & Chen, G. H. 1992, ApJ, 390, 550

Mohanty, S., & Basri, G. 2003, ApJ, 583, 451

Montes, D. et al. 1995, A&A, 294, 165M

Montes, D. et al. 1999, MNRAS, 305, 45

Montes, D. et al. 2000, A&AS, 146, 103M

Montes, D., Caballero, J. A., Alonso-Floriano, F. J., Cortés-Contreras, M., González-Álvarez, E., Hidalgo, D., Holgado, G., Martínez-Rodríguez, H., Sanz-Forcada, J., Proceedings of Cool Stars 18, The 18th Cool Stars, Stellar Systems and the Sun workshop (9 - 13 June 2014, Flagstaff, Arizona, USA)

Quirrenbach, A. et al. 2012, SPIE, 8446, E0R

Reid, I. N. et al. 1995, AJ, 110, 1838

Reid, I. N., & Hawley, S. L. : *New light on dark stars: red dwarfs, low-mass stars, brown dwarfs*. Springer, 2005.

Reiners, A. 2007, A&A, 467, 259

Reiners, A. et al. 2012, ApJ, 143, 93

Robertson, P. et al. 2013, ApJ, 764, 3

Scrijver, C. J., & Zwaan, C. : *Solar and stellar magnetic activity*. Cambridge Univ. Press, 2003.

Tonry, J., & Davis, M. 1979, ApJ, 84, 1511-1525

Torres, G. et al. 2006, A&A, 460, 695

White, R. J. et al. 2007, AJ, 133, 2524

Appendix: Figures

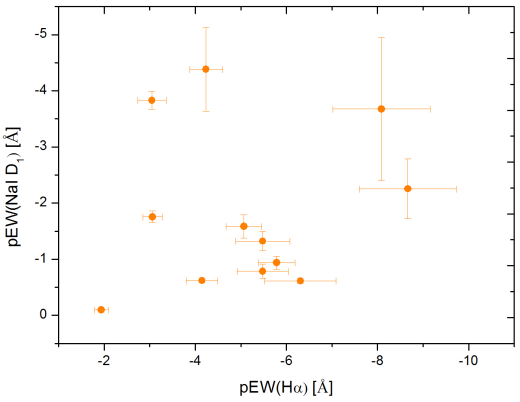

(a) $pEW(\text{Na I } D_1)$ vs $pEW(\text{H}\alpha)$.

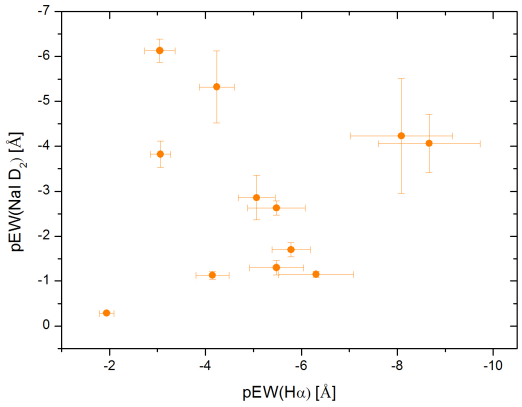

(b) $pEW(\text{Na I } D_2)$ vs $pEW(\text{H}\alpha)$.

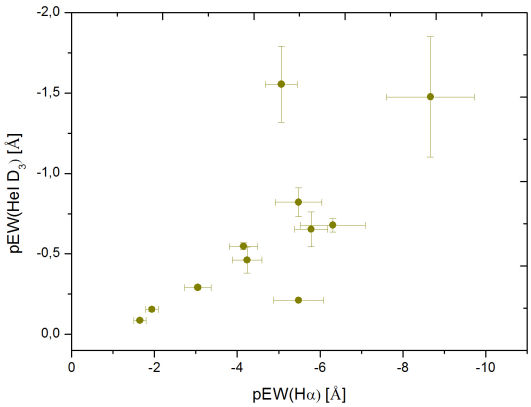

(c) $pEW(\text{He I } D_3)$ vs $pEW(\text{H}\alpha)$.

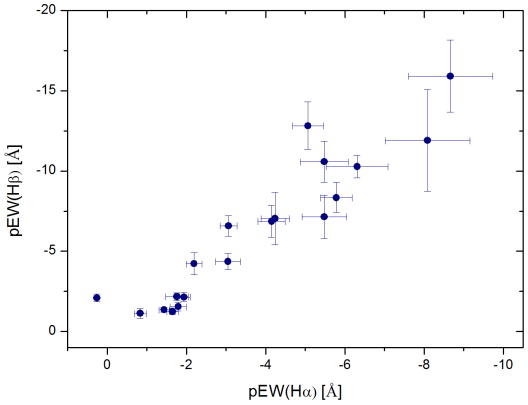

(d) $pEW(\text{H}\beta)$ vs $pEW(\text{H}\alpha)$.

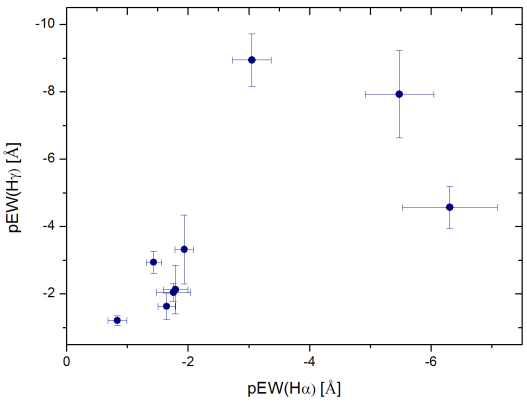

(e) $pEW(\text{H}\gamma)$ vs $pEW(\text{H}\alpha)$.

Figure 23: pEWs of the spectral lines vs $pEW(\text{H}\alpha)$.

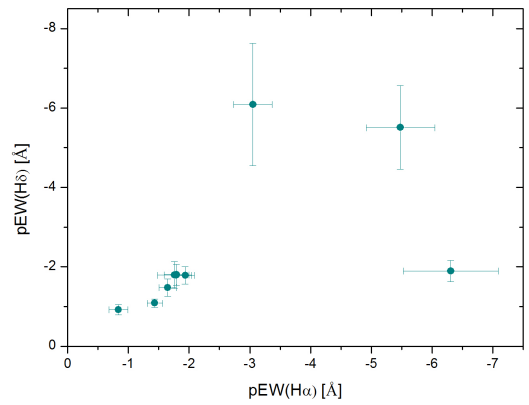

(a) $pEW(\mathrm{H}\delta)$ vs $pEW(\mathrm{H}\alpha)$.

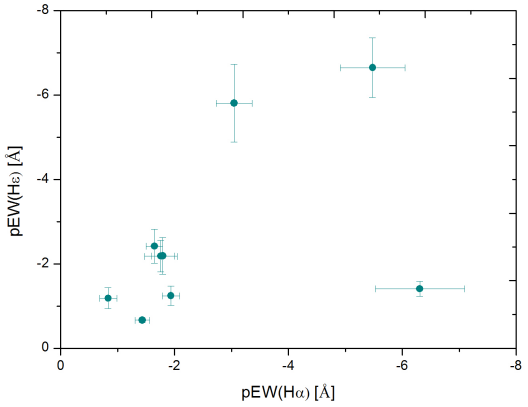

(b) $pEW(\mathrm{H}\epsilon)$ vs $pEW(\mathrm{H}\alpha)$.

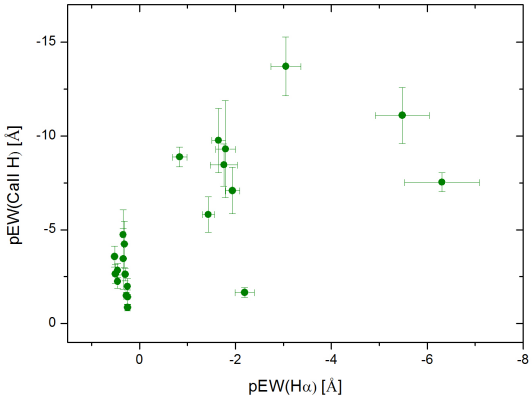

(c) $pEW(\mathrm{Ca\ II\ H})$ vs $pEW(\mathrm{H}\alpha)$.

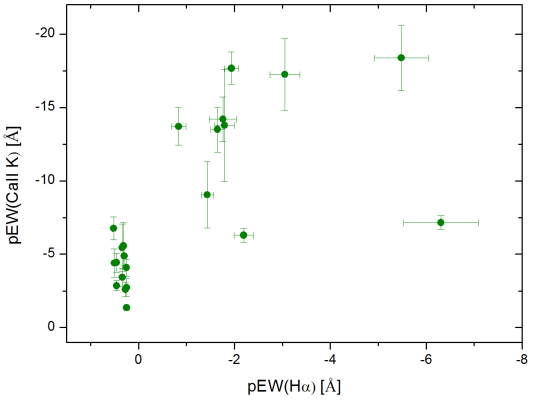

(d) $pEW(\mathrm{Ca\ II\ K})$ vs $pEW(\mathrm{H}\alpha)$.

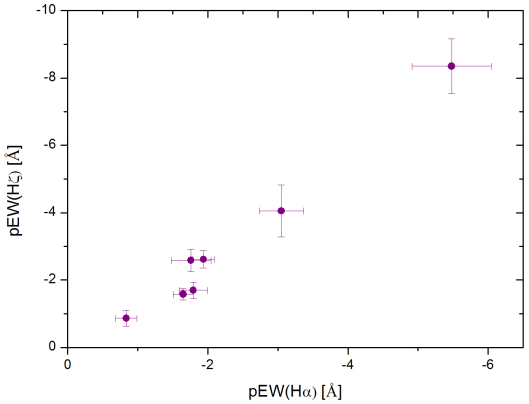

(e) $pEW(\mathrm{H}\zeta)$ vs $pEW(\mathrm{H}\alpha)$.

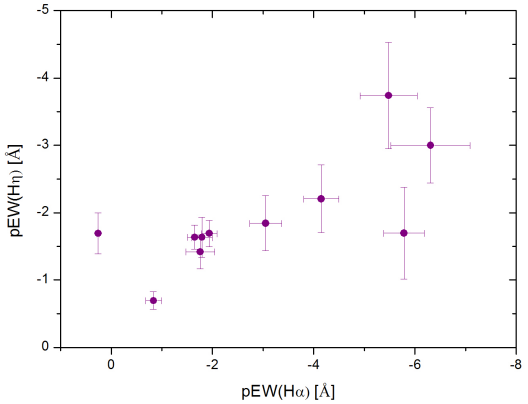

(f) $pEW(\mathrm{H}\eta)$ vs $pEW(\mathrm{H}\alpha)$.

Figure 24: pEWs of the spectral lines vs $pEW(\mathrm{H}\alpha)$ (continued).

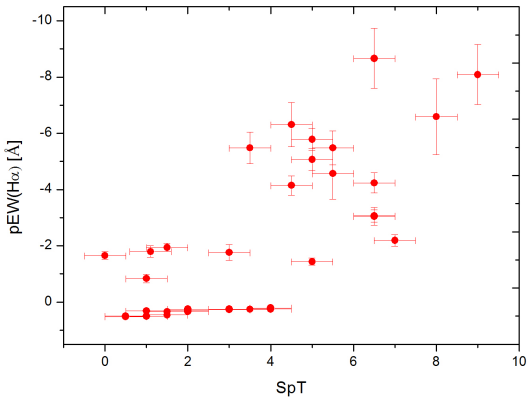

(a) pEW(Hα) vs SpT.

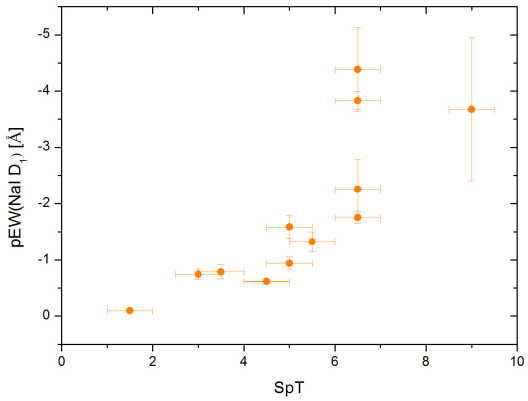

(b) pEW(Na I D_1) vs SpT.

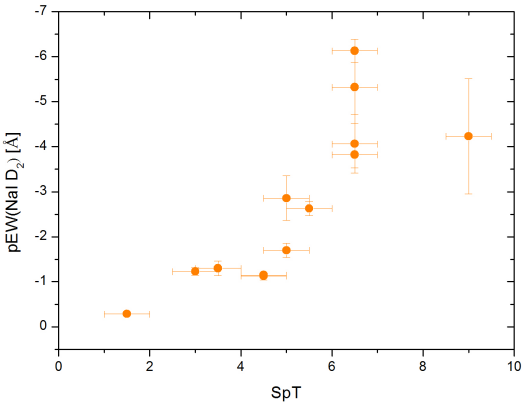

(c) pEW(Na I D_2) vs SpT.

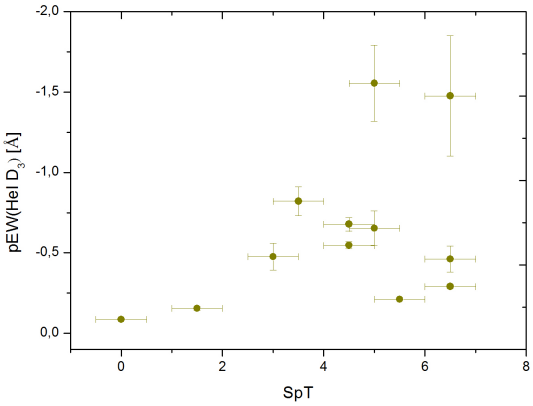

(d) pEW(He I D_3) vs SpT.

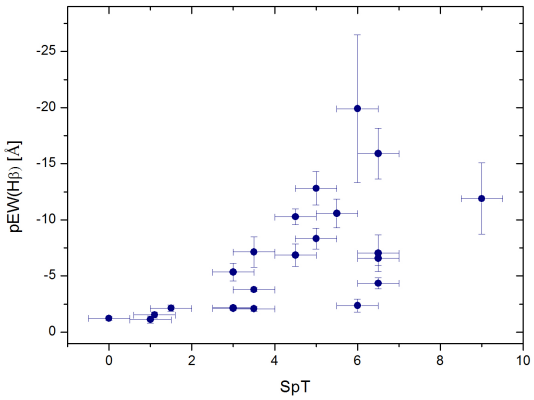

(e) pEW(Hβ) vs SpT.

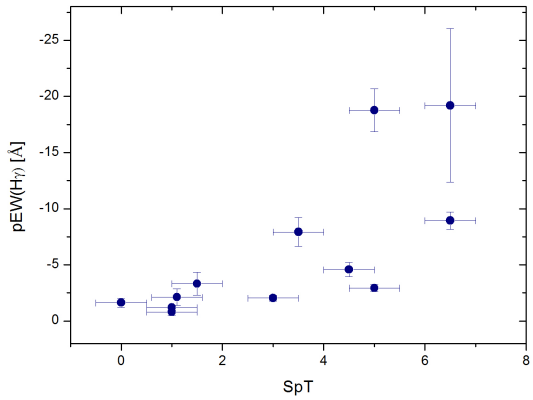

(f) pEW(Hγ) vs SpT.

Figure 25: pEWs vs spectral types.

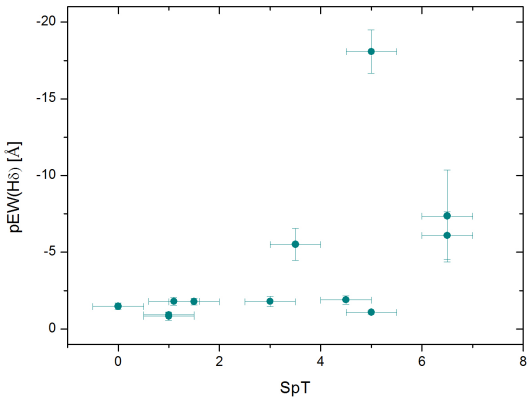

(a) pEW(Hδ) vs SpT.

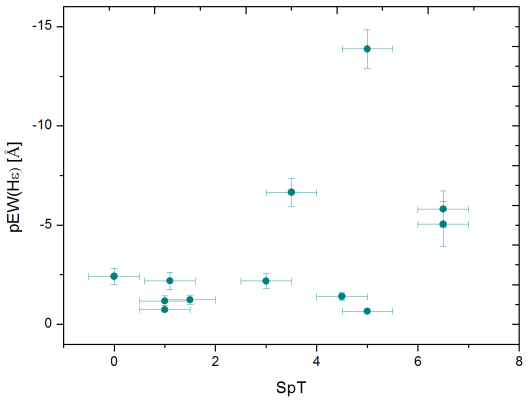

(b) pEW(Hϵ) vs SpT.

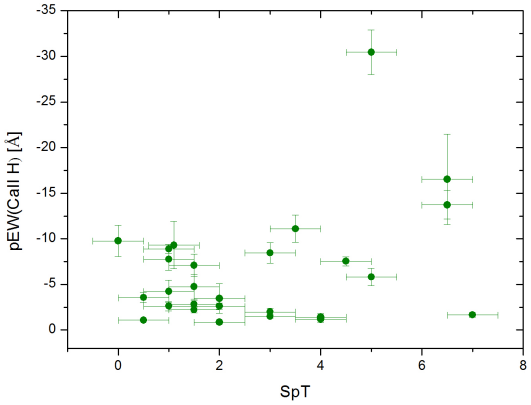

(c) pEW(Ca II H) vs SpT.

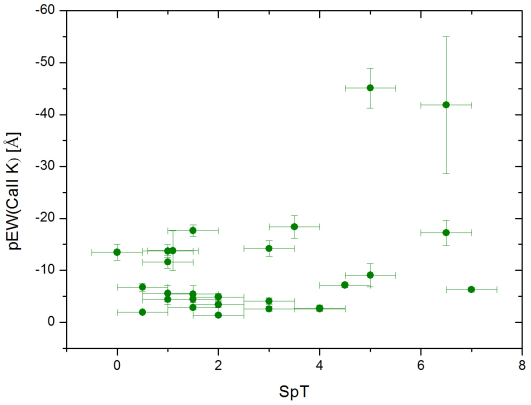

(d) pEW(Ca II K) vs SpT.

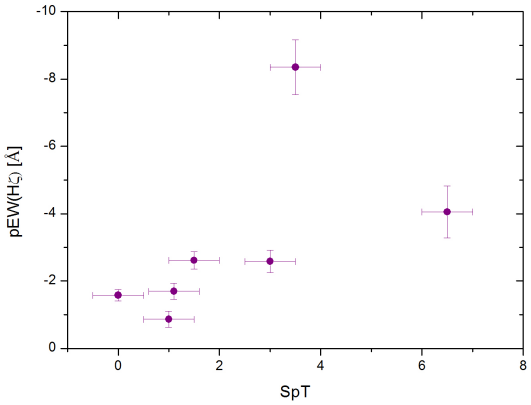

(e) pEW(Hζ) vs SpT.

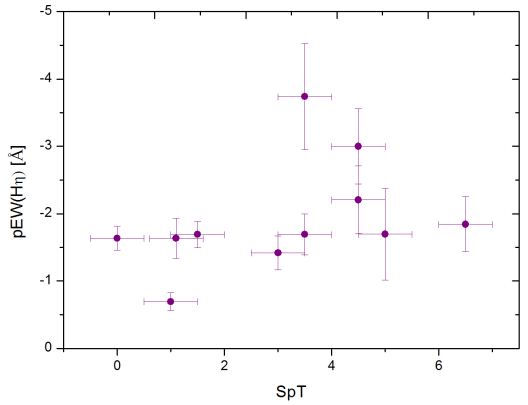

(f) pEW(Hη) vs SpT.

Figure 26: pEWs vs spectral types (continued).

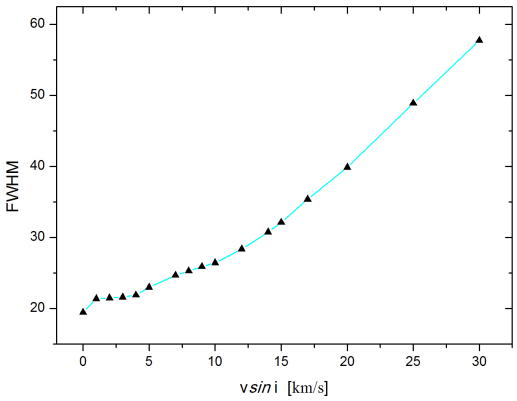

(a) J02442+255 (RED564 channel).

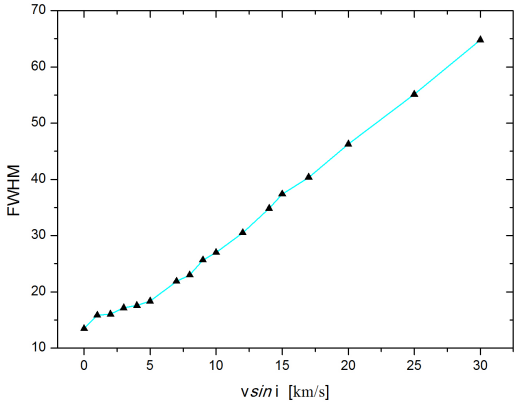

(b) J10289+008 (RED580 channel).

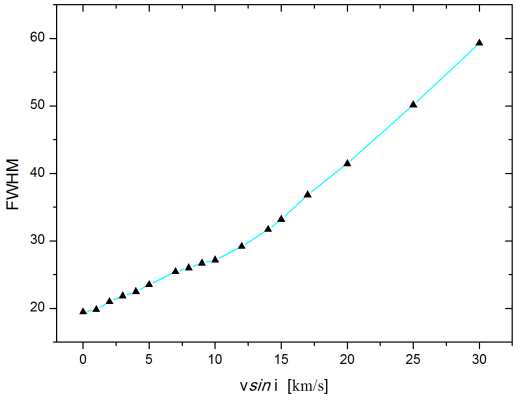

(c) J17052–050 (BLU437 channel).

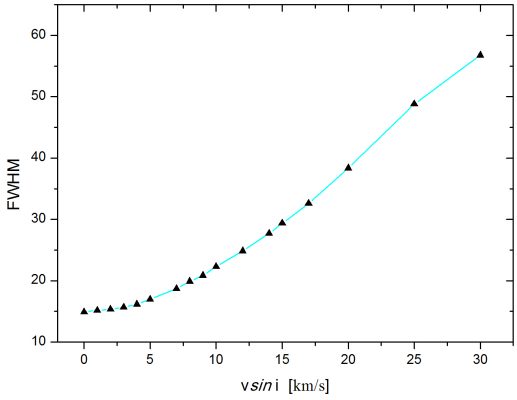

(d) J20574+223 (RED564 channel).

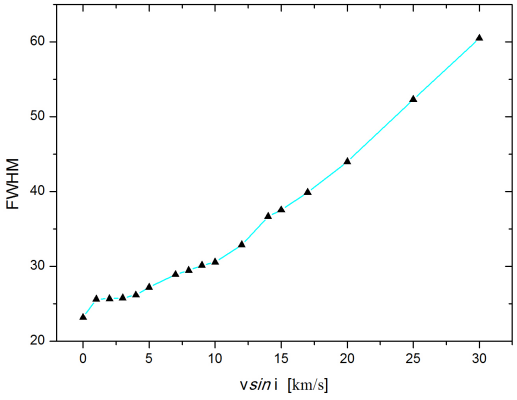

(e) J22021+014 (BLU437 channel).

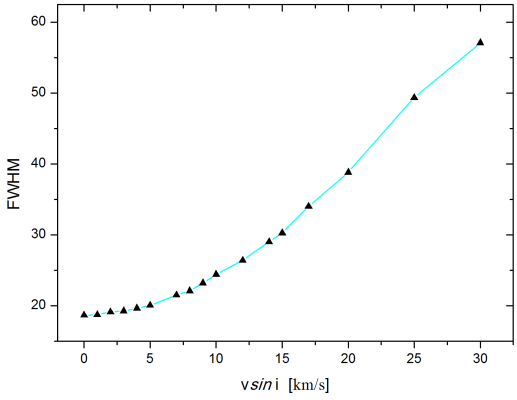

(f) J22559+057 (RED564 channel).

Figure 27: Calibration curves for the template stars.

Appendix: Tables

Table 10: Precise number of HARPS and UVES spectra for CARMENCITA sample.

Karmn	Name	α (J2000)	δ (J2000)	Class	# spec. HARPS	# spec. UVES
J00067–075	GJ 1002	00:06:43.26	-07:32:14.7	Alpha	5	5
J00286–066	GJ 1012	00:28:39.48	-06:39:48.1	Alpha	1	...
J01125–169	YZ Cet	01:12:30.53	-16:59:57.0	Alpha	12	...
J01433+043	GJ 70	01:43:20.15	+04:19:17.2	Alpha	8	...
J02002+130	TZ Ari	02:00:12.79	+13:03:11.2	Alpha	25	...
J02033–212	G 272-145	02:03:20.77	-21:13:42.7	Alpha	1	...
J02123+035	BD+02 348	02:12:20.91	+03:34:31.1	Alpha	19	...
J02362+068	BX Cet	02:36:15.36	+06:52:19.1	Alpha	251	...
J02442+255	VX Ari	02:44:15.38	+25:31:25.0	Alpha	...	14
J02530+168	Teegarden's Star	02:53:00.85	+16:52:53.3	Alpha	...	4
J03018–165S	BD–17 588 B	03:01:51.43	-16:35:35.7	Alpha	6	...
J03133+047	CD Cet	03:13:22.99	+04:46:29.4	Alpha	8	2
J03217–066	G 077-046	03:21:46.89	-06:40:24.2	Alpha	24	...
J03526+170	Wolf 227	03:52:41.69	+17:01:05.7	Alpha	5	...
J03574–011	BD–01 565B	03:57:28.92	-01:09:23.4	Alpha	1	...
J04153–076	omi02 Eri C	04:15:21.73	-07:39:17.4	Alpha	409	...
J04352–161	LP 775–031	04:35:16.13	-16:06:57.5	Alpha	...	8
J04376–110	BD–11 916	04:37:41.88	-11:02:19.8	Alpha	6	32
J04429+189	HD 285968	04:42:55.81	+18:57:28.5	Alpha	57	...
J04520+064	Wolf 1539	04:52:05.73	+06:28:35.6	Alpha	11	...
J04538–177	GJ 180	04:53:49.95	-17:46:23.5	Alpha	31	...
J05019–069	LP 656–038	05:01:57.47	-06:56:45.9	Alpha	7	...
J05033–173	LP 779–046	05:03:20.10	-17:22:24.5	Alpha	7	...
J05068–215E	BD–21 1074 A	05:06:49.47	-21:35:03.8	Alpha	5	10
J05280+096	Ross 41	05:28:00.15	+09:38:38.3	Alpha	8	...
J05314–036	HD 36395	05:31:27.35	-03:40:35.7	Alpha	103	...
J05322+098	V998 Ori	05:32:14.67	+09:49:15.0	Alpha	1	...
J05337+019	V371 Ori	05:33:44.81	+01:56:43.4	Alpha	1	...
J05348+138	Ross 46	05:34:52.12	+13:52:47.2	Alpha	11	...
J05365+113	V2689 Ori	05:36:30.99	+11:19:40.2	Alpha	19	...
J05366+112	2M J05363846+1117487	05:36:38.47	+11:17:48.8	Alpha	20	...
J05421+124	V1352 Ori	05:42:08.98	+12:29:25.3	Alpha	6	...
J06105–218	HD 42581 A	06:10:34.62	-21:51:52.2	Alpha	17	33
J06421+035	G 108-021	06:42:11.18	+03:34:52.7	Alpha	19	...
J06548+332	Wolf 294	06:54:49.03	+33:16:05.9	Alpha	...	28
J07274+052	Luyten's Star	07:27:24.50	+05:13:32.9	Alpha	63	...
J07287–032	GJ 1097	07:28:45.41	-03:17:52.4	Alpha	9	...
J07386–212	LP 763–001	07:38:40.89	-21:13:27.6	Alpha	7	...
J07446+035	YZ CMi	07:44:40.18	+03:33:09.0	Alpha	7	102
J08119+087	Ross 619	08:11:57.58	+08:46:22.1	Alpha	9	...
J08161+013	GJ 2066	08:16:07.98	+01:18:09.2	Alpha	8	...
J08298+267	DX Cnc	08:29:49.50	+26:46:34.8	Alpha	...	6
J08526+283	rho Cnc B	08:52:40.85	+28:18:58.9	Alpha	88	...
J08536–034	LP 666-009	08:53:36.20	-03:29:32.1	Alpha	...	12
J09011+019	Ross 625	09:01:10.49	+01:56:35.0	Alpha	1	...
J09161+018	RX J0916.1+0153	09:16:10.19	+01:53:08.8	Alpha	11	...

Table 10: (continued)

Karmn	Name	α (J2000)	δ (J2000)	Class	# spec. HARPS	# spec. UVES
J09161+018	GJ 1125	09:30:44.58	+00:19:21.4	Alpha	8	...
J09360–216	GJ 357	09:36:01.61	-21:39:37.1	Alpha	16	...
J09411+132	Ross 85	09:41:10.33	+13:12:34.4	Alpha	24	...
J09447–182	GJ 1129	09:44:47.31	-18:12:48.9	Alpha	3	...
J09511–123	BD–11 2741	09:51:09.64	-12:19:47.8	Alpha	1	...
J09531–036	GJ 372	09:53:11.78	-03:41:24.0	Alpha	1	...
J10122–037	AN Sex	10:12:17.69	-03:44:44.1	Alpha	33	...
J10167–119	GJ 386	10:16:46.00	-11:57:41.3	Alpha	6	...
J10251–102	BD–09 3070	10:25:10.88	-10:13:43.4	Alpha	34	...
J10289+008	BD+01 2447	10:28:55.55	+00:50:27.5	Alpha	29	3
J10396–069	GJ 399	10:39:40.61	-06:55:25.6	Alpha	7	...
J10482–113	LP 731–058	10:48:12.58	-11:20:08.2	Alpha	...	15
J10508+068	EE Leo	10:50:52.01	+06:48:29.3	Alpha	4	...
J10564+070	CN Leo	10:56:28.86	+07:00:52.8	Alpha	3	313
J11026+219	DS Leo	11:02:38.33	+21:58:01.7	Alpha	9	...
J11033+359	HD 95735	11:03:20.24	+35:58:11.8	Alpha	...	19
J11421+267	Ross 905 b	11:42:10.96	+26:42:25.1	Alpha	142	...
J11467–140	GJ 443	11:46:42.82	-14:00:50.5	Alpha	13	...
J11477+008	FI Vir	11:47:44.40	+00:48:16.4	Alpha	6	10 (+6)
J12100–150	LP 734–032	12:10:05.60	-15:04:15.7	Alpha	7	(+6)
J12111–199	LTT 4562	12:11:11.80	-19:57:37.7	Alpha	8	...
J12142+006	GJ 1154 A	12:14:16.54	+00:37:26.3	Alpha	5	...
J12189+111	GL Vir	12:18:59.40	+11:07:33.9	Alpha	...	18
J12248–182	Ross 695	12:24:52.43	-18:14:30.3	Alpha	15	...
J12350+098	GJ 476	12:35:00.70	+09:49:42.5	Alpha	11	...
J12388+116	Wolf 433	12:38:52.42	+11:41:46.2	Alpha	5	...
J12479+097	Wolf 437	12:47:56.64	+09:45:05.0	Alpha	4	...
J13005+056	FN Vir	13:00:33.51	+05:41:08.1	Alpha	...	6
J13168+170	HD 115404B	13:16:51.56	+17:01:00.1	Alpha	...	2
13293+114	GJ 513	13:29:21.31	+11:26:26.5	Alpha	7	...
J13299+102	BD+11 2576	13:29:59.79	+10:22:37.6	Alpha	8	...
J13457+148	HD 119850	13:45:43.54	+14:53:31.8	Alpha	29	11
J13458–179	LP 798–034	13:45:50.75	-17:58:04.8	Alpha	8	...
J13582+125	Ross 837	13:58:13.93	+12:34:43.8	Alpha	1	...
J14010–026	HD 122303	14:01:03.25	-02:39:18.1	Alpha	34	...
J14294+155	Ross 130	14:29:29.72	+15:31:57.9	Alpha	8	...
J14310–122	Wolf 1478	14:31:01.20	-12:17:45.2	Alpha	8	...
J14342–125	HN Lib	14:34:16.83	-12:31:10.7	Alpha	7	6
J14524+123	G 066–037	14:52:28.54	+12:23:33.0	Alpha	13	...
J15013+055	G 015–002	15:01:20.11	+05:32:55.4	Alpha	6	...
J15095+031	Ross 1047	15:09:35.59	+03:10:00.8	Alpha	8	...
J15191–127	LP 742–061	15:19:11.82	-12:45:06.2	Alpha	6	...
J15194–077	HO Lib	15:19:26.89	-07:43:20.1	Alpha	200	...
J15474–108	LP 743–031	15:47:24.64	-10:53:47.1	Alpha	3	...
J15598–082	BD–07 4156	15:59:53.37	-08:15:11.4	Alpha	16	12
J16303–126	V2306 Oph	16:30:18.09	-12:39:43.4	Alpha	23	...
J16327+126	GJ 1203	16:32:45.25	+12:36:46.0	Alpha	6	...
J16555–083	vB 8	16:55:35.29	-08:23:40.1	Alpha	7	14

Table 10: (continued)

Karmn	Name	α (J2000)	δ (J2000)	Class	# spec. HARPS	# spec. UVES
J16570–043	LP 686-027	16:57:05.71	-04:20:56.0	Alpha	1	...
J17052–050	Wolf 636	17:05:13.84	-05:05:38.6	Alpha	19	12
J17136–084	V2367 Oph	17:13:40.48	-08:25:14.4	Alpha	1	...
J17166+080	GJ 2128	17:16:40.97	+08:03:30.2	Alpha	6	...
J17303+055	BD+05 3409	17:30:22.73	+05:32:54.7	Alpha	11	...
J17378+185	BD+18 3421	17:37:53.3	+18:35:29.5	Alpha	6	...
J17578+046	Barnard's Star	17:57:48.49	+04:41:40.5	Alpha	156	...
J18051–030	HD 165222	18:05:07.56	-03:01:52.4	Alpha	12	...
J18075–159	GJ 1224	18:07:32.93	-15:57:46.5	Alpha	4	...
J18363+136	Ross 149	18:36:19.23	+13:36:26.2	Alpha	1	...
J18409–133	BD–13 5069	18:40:57.33	-13:22:45.6	Alpha	21	...
J18427+139	V816 Her	18:42:44.99	+13:54:16.8	Alpha	3	...
J18580+059	BD+05 3993	18:58:00.14	+05:54:29.7	Alpha	12	...
J19098+176	GJ 1232	19:09:50.98	+17:40:07.4	Alpha	4	...
J19169+051N	V1428 Aql	19:16:55.26	+05:10:08.6	Alpha	14	1
J19169+051S	V1298 Aql (vB 10)	19:16:57.62	+05:09:02.2	Alpha	14	1
J20405+154	GJ 1256	20:40:33.64	+15:29:57.2	Alpha	6	...
J20525–169	LP 816-060	20:52:33.04	-16:58:29.0	Alpha	7	...
J22021+014	BD+00 4810	22:02:10.26	+01:24:00.6	Alpha	31	14
J22096–046	BD–05 5715	22:09:40.30	-04:38:26.8	Alpha	36	...
J22137–176	LP 819-052	22:13:42.78	-17:41:08.2	Alpha	6	...
J22231–176	LP 820-012	22:23:06.97	-17:36:25.0	Alpha	3	...
J22330+093	BD+08 4887	22:33:02.25	+09:22:41.1	Alpha	5	...
J22532–142	IL Aqr	22:53:16.72	-14:15:48.9	Alpha	59	5
J22565+165	HD 216899	22:56:34.97	+16:33:13.0	Alpha	12	2
J23216+172	LP 462-027	23:21:37.52	+17:17:28.5	Alpha	7	...
J23492+024	BR Psc	23:49:12.56	+02:24:03.8	Alpha	35	...
J00158+135	GJ 12	00:15:49.20	+13:33:21.9	Beta	6	...
J00182+102	GJ 16	00:18:16.59	+10:12:10.1	Beta	6	...
J01066+152	GJ 1030	01:06:41.52	+15:16:22.9	Beta	1	...
J01384+006	G 071–024	01:38:29.98	+00:39:05.9	Beta	1	...
J02096–143	LP 709–040	02:09:36.09	-14:21:32.1	Beta	2	...
J03507–060	GJ 1065	03:50:44.32	-06:05:40.0	Beta	5	...
J04595+017	V1005 Ori	04:59:34.83	+01:47:00.7	Beta	1	10
J05298–034	Wolf 1450	05:29:52.05	-03:26:29.6	Beta	10	...
J06422+035	G 108–022	06:42:13.34	+03:35:31.1	Beta	19	...
J07403–174	LP 783–002	07:40:19.22	-17:24:44.9	Beta	...	4
J08314–060	LP 665–022	08:31:27.23	-06:02:12.5	Beta	21	...
J09023+084	NLTT 20817	09:02:19.88	+08:28:06.4	Beta	6	...
J09425–192	LP 788–024	09:42:35.73	-19:14:04.6	Beta	11	...
J10584–107	LP 731–076	10:58:28.00	-10:46:30.5	Beta	...	1
J11541+098	Ross 119	11:54:07.88	+09:48:22.7	Beta	11	...
J12016–122	LTT 4484	12:01:40.80	-12:13:53.7	Beta	1	...
J12112–199	LP 794–031	12:11:16.98	-19:58:21.4	Beta	8	...
J13526+144	G 150–046	13:52:36.20	+14:25:20.9	Beta	2	...
J13526+144	LP 806–008	16:48:45.97	-15:44:19.9	Beta	7	...
J17160+110	BD+11 3149	17:16:00.63	+11:03:27.4	Beta	6	...

Table 10: (continued)

Karmn	Name	α (J2000)	δ (J2000)	Class	# spec. HARPS	# spec. UVES
J18240+016	G 021–013	18:24:05.18	+01:41:16.1	Beta	1	...
J18451+063	TYC 460–624–1	18:45:10.27	+06:20:15.8	Beta	...	4
J20407+199	GJ 797B	20:40:44.50	+19:54:02.3	Beta	57	...
J20429–189	BD–19 5899	20:42:57.09	-18:55:04.8	Beta	30	...
J21092–133	Wolf 918	21:09:17.41	-13:18:08.0	Beta	5	...
J22058–119	BD–12 6174	22:05:51.31	-11:54:50.7	Beta	33	...
J00176–086	BD–09 40	00:17:40.89	-08:40:55.9	Gamma	1	...
J00201–170	LP 764–108	00:20:08.38	-17:03:40.9	Gamma	43	...
J00515–229	HD 4967 B	00:51:35.16	-22:54:30.8	Gamma	2	...
J01182–128	GJ 56.1	01:18:15.99	-12:53:58.1	Gamma	10	...
J01324–219	CD–22 526	01:32:26.26	-21:54:17.3	Gamma	1	...
J01518–108	Ross 555	01:51:48.65	-10:48:12.0	Gamma	2	...
J02020+039	Wolf 109 B	02:02:03.47	+03:56:42.2	Gamma	1	...
J02022+103	LP 469–067	02:02:16.21	+10:20:13.7	Gamma	...	5
J02164+135	LP 469–206	02:16:29.78	+13:35:13.7	Gamma	...	4
J02289+120	R78b 140	02:28:54.66	+12:05:20.9	Gamma	1	...
J02438–088	Wolf 1132	02:43:53.17	-08:49:44.9	Gamma	2	...
J02581–128	LP 711–032	02:58:10.21	-12:53:06.7	Gamma	8	...
J03102+059	EK Cet	03:10:15.47	+05:54:31.1	Gamma	9	...
J03233+116	G 005–032	03:23:22.41	+11:41:13.4	Gamma	1	...
J03317+143	GJ 143.3	03:31:47.12	+14:19:19.4	Gamma	1	...
J03479+027	Ross 588	03:47:58.09	+02:47:16.2	Gamma	6	...
J03544–091	StKM 1–430	03:54:25.62	-09:09:31.6	Gamma	16	...
J04403–055	LP 655–048	04:40:23.25	-05:30:08.3	Gamma	...	9
J04407+022	StKM 1–502	04:40:42.49	+02:13:52.2	Gamma	11	...
J04471+021	G 082–048	04:47:11.75	+02:09:39.7	Gamma	7	...
J04559+046	HD 31412B	04:55:54.46	+04:40:16.4	Gamma	...	[6]
J05018+037	StKM 1–539	05:01:50.57	+03:45:55.1	Gamma	5	...
J05060+043	G 084–036	05:06:04.02	+04:20:14.3	Gamma	9	...
J05151–073	NLTT 14750	05:15:08.05	-07:20:48.6	Gamma	8	...
J05472–000	StKM 1–578	05:47:17.97	-00:00:48.7	Gamma	1	...
J06218–227	BD–22 3005	06:21:53.85	-22:43:24.2	Gamma	21	...
J07590+153	LP 424–004	07:59:05.87	+15:23:29.5	Gamma	11	...
J08313–060	LP 665–021	08:31:21.63	-06:02:01.7	Gamma	21	...
J09050+028	LP 546–48	09:05:04.43	+02:50:03.1	Gamma	16	...
J09238+001	LP 607–039	09:23:52.56	+00:08:17.8	Gamma	1	...
J10243+119	StKM 1–852	10:24:20.17	+11:57:20.7	Gamma	1	...
J10456–191	BD–18 3019	10:45:39.31	-19:06:50.9	Gamma	7	...
J11057+102	LP 491–060	11:05:43.16	+10:14:09.3	Gamma	1	...
J11152–181	LP 792–009	11:15:15.50	-18:07:34.8	Gamma	9	...
J11237+085	Wolf 386	11:23:44.56	+08:33:48.4	Gamma	7	...
J11532–073	GJ 452	11:53:16.09	-07:22:27.3	Gamma	8	...
J11551+009	Ross 129	11:55:07.21	+00:58:25.7	Gamma	2	...
J11575+118	Ross 122	11:57:32.78	+11:49:39.8	Gamma	2	...
J13215+037	LP 557–059	13:21:35.24	+03:45:55.2	Gamma	3	...
J13388–022	Ross 488	13:38:53.45	-02:15:47.1	Gamma	7	...
J13415+148	LTT 18344	13:41:31.89	+14:49:26.7	Gamma	3	...

Table 10: (continued)

Karmn	Name	α (J2000)	δ (J2000)	Class	# spec. HARPS	# spec. UVES
J14023+136	MCC 150	14:02:19.61	+13:41:22.9	Gamma	7	...
J14170+105	LP 499–059	14:17:04.88	+10:35:35.9	Gamma	6	...
J14249+088	LP 500–019	14:24:55.99	+08:53:15.6	Gamma	6	...
J14548+099	Ross 1028b	14:54:53.47	+09:56:36.4	Gamma	8	...
J15501+009	Wolf 587	15:50:11.21	+00:57:32.6	Gamma	1	...
J16204–042	LP 685–051	16:20:24.77	-04:16:02.3	Gamma	24	...
J16328+098	G 138–040	16:32:52.85	+09:50:26.0	Gamma	2	...
J17027–060	BD–05 4394	17:02:49.59	-06:04:06.4	Gamma	7	...
J17153+049	GJ 1214	17:15:18.94	+04:57:49.7	Gamma	21	...
J17183–017	MCC 791	17:18:21.73	-01:46:53.6	Gamma	9	...
J17242–043	LP 687–031	17:24:16.95	-04:21:52.1	Gamma	1	...
J17388+080	G 139–050	17:38:51.25	+08:01:35.3	Gamma	1	...
J17432–185	Ross 133	17:43:17.55	-18:31:17.9	Gamma	1	...
J18402–104	Ross 719	18:40:17.84	-10:27:55.0	Gamma	1	...
J18500+030	Ross 142	18:50:00.83	+03:05:17.4	Gamma	1	...
J18571+075	LP 571–080	18:57:10.54	+07:34:17.1	Gamma	1	...
J18596+079	BD+07 3922	18:59:38.60	+07:59:14.0	Gamma	3	...
J19106+015	G 022–017	19:10:38.55	+01:32:10.5	Gamma	1	...
J19510+104	omi Aql B	19:51:00.68	+10:24:40.1	Gamma	32	[6]
J19582+020	LP 634–002	19:58:15.72	+02:02:15.2	Gamma	1	...
J20038+059	GJ 1248	20:03:50.98	+05:59:44.0	Gamma	1	...
J20574+223	Wolf 3273	20:57:25.38	+22:21:45.7	Gamma	...	4
J22524+099	sig Peg B	22:52:29.77	+09:54:04.3	Gamma	166	...
J22559+057	LP 581–036	22:55:56.83	+05:45:17.9	Gamma	...	10
J23064–050	2MUCD 12171	23:06:29.28	-05:02:28.6	Gamma	...	12
J23142–196S	BD–20 6558B	23:14:16.43	-19:38:46.2	Gamma	3	...
J23142–196N	BD–20 6558	23:14:16.60	-19:38:39.3	Gamma	3	...
J01114+154	LP 467–016 AB	01:11:25.42	+15:26:21.5	Delta	...	4
J01178+054	NLTT 4318	01:17:53.26	+05:28:25.7	Delta	5	...
J01390–179	BL Cet + UV Cet	01:39:01.20	-17:57:02.7	Delta	...	14
J03018–165N	BD–17 588 AC	03:01:51.08	-16:35:30.7	Delta	6	...
J03075–039	LP 652–005 AB	03:07:33.83	-03:58:16.7	Delta	14	...
J04376–024	StKM 1–497 Cab	04:37:37.46	-02:29:28.2	Delta	4	6
J04404–091	BD–09 956 AB	04:40:29.28	-09:11:45.8	Delta	5	...
J05068–215W	BD–21 1074 BC	05:06:49.92	-21:35:09.2	Delta	5	10
J05402+126	V1402 Ori AB	05:40:16.09	+12:39:00.8	Delta	1	...
J06171+051	HD 43587 BC	06:17:10.65	+05:07:02.4	Delta	3	...
J06293–028	V577 Mon AB	06:29:23.39	-02:48:50.0	Delta	5	...
J06523–051	BD–05 1844Bab	06:52:18.04	-05:11:24.1	Delta	6	...
J08105–138	GJ 297.2B	08:10:34.29	-13:48:51.4	Delta	201	...
J08126–215	GJ 300 AB	08:12:40.88	-21:33:05.7	Delta	24	8
J08570+116	BD+12 1944 AB	08:57:04.68	+11:38:49.1	Delta	1	...
J08582+197	EI Cnc AB	08:58:15.19	+19:45:47.1	Delta	...	10
J08589+084	NLTT 20670	08:58:56.33	+08:28:25.9	Delta	...	4
J09313–134	Ross 440	09:31:19.37	-13:29:19.3	Delta	1	...
J10196+198	AD Leo AB	10:19:36.35	+19:52:12.2	Delta	40	16
J11214–204	BD–19 3242B	11:21:26.56	-20:27:09.5	Delta	1	...

Table 10: (continued)

Karmn	Name	α (J2000)	δ (J2000)	Class	# spec. HARPS	# spec. UVES
J12168+029	GJ 1155 AB	12:16:51.91	+02:58:04.7	Delta	...	6
J12289+084	Wolf 414 AB	12:28:57.60	+08:25:31.6	Delta	8	...
J12288–106N	Ross 948 A	12:28:52.98	-10:39:50.8	Delta	1	...
J12288–106S	Ross 948 B	12:28:53.16	-10:39:48.8	Delta	1	...
J13007+123	DT Vir AB	13:00:46.66	+12:22:32.6	Delta	2	...
J14544+161	CE Boo A	14:54:29.23	+16:06:04.0	Delta	6	2
J14574–214	KX Lib BC	14:57:27.88	-21:24:52.7	Delta	411	[8]
J16066+083	GJ 611.3 AB	16:06:41.18	+08:23:18.2	Delta	7	...
J16302–146	LP 745–051	16:30:13.14	-14:39:49.5	Delta	1	...
J16554–083N	GJ 643 Dab	16:55:25.27	-08:19:20.8	Delta	7	17 (+12)
J16554–083S	V1054 Oph ABab	16:55:28.81	-08:20:10.3	Delta	7	3
J17118–018	LP 627–009	17:11:52.34	-01:51:05.7	Delta	1	...
J17430+057	G 140–009 AB	17:43:00.82	+05:47:21.6	Delta	3	...
J17570+157	LP 449–006 AB	17:57:03.56	+15:46:43.2	Delta	1	...
J18387–144	GJ 2138	18:38:44.75	-14:29:25.0	Delta	1	...
J18480–145	G 155–042	18:48:01.29	-14:34:50.8	Delta	1	...
J18548+109	V1436 Aql B	18:54:53.81	+10:58:43.5	Delta	1	...
J18554+084	V1285 Aql AB	18:55:27.41	+08:24:09.0	Delta	1	8 (+12)
J19093–147	Ross 727	19:09:19.89	-14:44:55.2	Delta	1	...
J19205–076	GJ 754.1B	19:20:33.46	-07:39:43.6	Delta	1	[8]
J19220+070	GJ 1236	19:22:02.07	+07:02:31.0	Delta	8	...
J22361–008	HD 214100	22:36:09.67	-00:50:29.8	Delta	10	...
J22387–206N	FL Aqr	22:38:45.31	-20:36:51.9	Delta	3	...
J22387–206S	FK Aqr	22:38:45.60	-20:37:16.1	Delta	3	...

[ ] Primary companions.

( ) Unavailable spectra.

Table 11: UVES channels for our sample.

Karmn	Channel											
	BLU346	BLU390	BLU437	BLU445	RED564	RED580	RED600	RED760	RED800	RED830	RED840	RED860
J00067–075	...	...	...	...	...	...	...	...	...	...	Yes	...
J02442+255	Noise	...	Yes	...	...	Noise	...	...	...	...	...	Yes
J02530+168	...	...	...	...	...	...	...	...	...	...	Yes	...
J03133+047	...	...	Yes	...	...	...	...	Yes	...	...	...	...
J04352–161	...	Noise	Yes	...	...	...	...	...	...	Yes	...	...
J04376–110	...	...	Yes	...	...	...	Yes	Yes	...	...	...	...
J05068–215E	...	Yes	...	...	...	Yes	...	...	...	...	...	...
J06105–218	Noise	...	...	...	Bad	...	Yes	...	...	...	...	...
J06548+332	...	...	Yes	...	...	...	...	Yes	...	...	...	...
J07446+035	Noise	Noise	...	...	Noise	...	...	...	...	Yes	...	...
J08298+267	Noise	...	...	...	Yes	...	...	...	...	...	...	...
J08536–034	Noise	...	...	...	Yes	...	...	...	...	...	...	Yes
J10289+008	...	Yes	...	...	...	Yes	...	...	...	...	...	...
J10482–113	Yes	...	Yes	...	...	...	...	Yes	...	...	...	Yes
J10564+070	Yes	...	Yes	...	Yes	...	...	...	...	Yes	...	...
J11033+359	Noise	...	Yes	...	...	Noise	...	...	...	...	...	Yes
J11477+008	...	...	C. rays	...	...	...	...	...	...	C. rays	...	...
J12189+111	Yes	...	C. rays	...	Yes	...	...	...	...	Yes	...	...
J13005+056	Yes	...	...	...	Yes	...	...	...	...	...	...	...
J13168+170	...	...	...	...	...	Yes	...	...	...	...	...	...
J13457+148	...	Yes	...	...	...	Yes	...	...	...	...	...	...
J14342–125	...	...	...	...	...	...	...	...	Yes	...	...	...
J15598–082	...	...	Yes	...	...	...	...	...	...	Yes	...	...
J16555–083	Noise	...	...	...	Yes	...	...	...	...	...	...	...
J17052–050	...	...	Yes	...	...	...	...	...	...	Yes	...	...
J19169+051N	...	...	...	...	...	...	...	...	...	...	...	Yes
J19169+051S	...	...	...	...	...	...	...	...	...	...	...	Yes
J22021+014	...	...	Yes	...	...	...	...	Yes	...	...	...	...
J22532–142	...	...	Yes	...	...	Yes	...	Yes	...	...	...	Yes
J22565+165	...	...	...	Yes	...	...	...	Bad	...	...	...	...

Table 11: (continued)

Karmn	Channel											
	BLU346	BLU390	BLU437	BLU445	RED564	RED580	RED600	RED760	RED800	RED830	RED840	RED860
J04595+017	...	Yes	...	...	...	Yes	...	...	...	...	...	...
J07403–174	...	Noise	...	...	Yes	...	...	...	...	...	...	...
J10584–107	Noise	...	...	...	...	...	...	...	...	...	...	...
J18451+063	...	Yes	...	...	...	Noise	...	...	...	...	...	...
J02022+103	...	...	...	...	...	...	...	...	...	...	Bad	...
J02164+135	...	...	...	...	...	...	...	...	...	...	Yes	...
J04403–055	...	...	C. rays	...	...	...	...	...	...	...	...	Yes
J04559+046	...	Prim. comp.	...	...	...	...	...	Prim. comp.	...	...	...	...
J19510+104	...	Prim. comp.	...	...	...	...	...	Prim. comp.	...	...	...	...
J20574+223	...	Yes	...	...	Yes	...	...	...	...	...	...	...
J22559+057	...	Yes	...	...	Yes	...	...	...	...	...	...	...
J23064–050	...	...	C. rays	...	...	...	...	...	...	...	Yes	...
J01114+154	...	...	...	...	...	...	...	...	...	...	Yes	...
J01390–179	Yes	...	Yes	...	...	Yes	...	...	...	...	...	Yes
J04376–024	...	Yes	...	...	...	Yes	...	...	...	...	...	...
J05068–215W	...	Yes	...	...	...	Yes	...	...	...	...	...	...
J08126–215	...	...	Yes	...	...	...	...	...	...	...	...	Yes
J08582+197	Noise	...	...	...	Yes	...	...	...	...	...	...	...
J08589+084	Yes	...	...	...	Yes	...	...	...	...	...	...	...
J10196+198	Yes	...	...	...	Yes	...	...	...	...	...	...	...
J12168+029	...	Bad	...	...	C. rays	...	...	...	...	...	...	...
J14544+161	...	...	Yes	...	...	...	...	...	...	Yes	...	...
J14574–214	...	Prim. comp.	...	...	...	Prim. comp.	...	...	Prim. comp.	...	...	...
J16554–083N	Yes	...	Yes	...	Yes	...	...	...	...	Yes	...	...
J16554–083S	Yes	...	...	...	Yes	...	...	...	...	...	...	...
J18554+084	...	...	Yes	...	...	...	...	...	...	Yes	...	...
J19205–076	...	Prim. comp.	...	...	Prim. comp.	...	...	...	...	...	...	Prim. comp.

Table 12: pEWs of Balmer series.

Karmn	pEW [Å]						
	Hη	Hζ	Hϵ	Hδ	Hγ	Hβ	Hα
J02442+255			...	...	...	...	0.270 ± 0.006
J03133+047	...	...	-0.668 ± 0.053	-1.09 ± 0.11	-2.94 ± 0.32	-1.35 ± 0.14	-1.43 ± 0.13^b
J04352–161	...	...	...	...	...	-4.21 ± 0.68	-2.19 ± 0.20
J04376–110^a	...	...	...	...	...	...	0.456 ± 0.013
J04376–110^a							0.448 ± 0.012
J05068–215E	-1.69 ± 0.20	-2.62 ± 0.26	-1.25 ± 0.23	-1.79 ± 0.22	-3.3 ± 1.0	-2.14 ± 0.28	-1.94 ± 0.15^b
J06105–218							0.499 ± 0.014
J06548+332	...	...	...	...	...	...	0.251 ± 0.027
J07446+035	-3.00 ± 0.56	...	-1.41 ± 0.18	-1.89 ± 0.27	-4.57 ± 0.63	-10.28 ± 0.70	-6.31 ± 0.78^b
J08298+267	...	...				-6.58 ± 0.65	-3.06 ± 0.22^b
J08536–034						-11.9 ± 3.2	-8.1 ± 1.1^b
J10289+008	...	...	...	...	...	...	0.297 ± 0.018
J10482–113^a	-5.8 ± 2.6						
J10482–113^a	-1.84 ± 0.41	-4.06 ± 0.77	-5.81 ± 0.92	-6.09 ± 1.54	-8.95 $\pm$ 0.77	-4.35 ± 0.50	-3.05 ± 0.32
J10564+070^a	-6.96 ± 0.97						
J10564+070^a	-3.0 ± 1.3	-13.1 ± 5.2	-5.0 ± 1.1	-7.4 ± 3.0	-19.2 ± 6.8	-10.4 ± 2.9	
J10564+070^a						-15.9 ± 2.2	-8.7 ± 1.0^b
J10564+070^a							-7.7 ± 1.2^b
J11033+359	...	...	...	...	...	...	...
J12189+111	-1.70 ± 0.68	...	...	...	...	-8.34 ± 0.93	-5.78 ± 0.40^b
J13005+056	-2.21 ± 0.50	...	...	...	...	-6.87 ± 0.99	-4.15 ± 0.34^b
J13168+170						...	
J13457+148	...	...	...	...	...	...	0.456 ± 0.008
J14342–125							0.207 ± 0.010
J15598–082	...	...	...	...	...	...	0.314 ± 0.016
J16555–083						-7.0 ± 1.6	-4.24 ± 0.36^b
J17052–050	...	...	...	...	...	...	0.339 ± 0.018
J22021+014	...	...	...	...	...	...	0.518 ± 0.026
J22532–142	...	...	...	...	...	...	0.248 ± 0.013
J22565+165	...	...	...	...	...	...	0.341 ± 0.040

Table 12: (continued)

Karmn	pEW [Å]						
	Hη	Hζ	Hϵ	Hδ	Hγ	Hβ	Hα
J04595+017	-1.64 ± 0.18	-1.58 ± 0.17	-2.42 ± 0.41	-1.48 ± 0.22	-1.63 ± 0.40	-1.23 ± 0.18	-1.65 ± 0.14^{b}
J07403–174	...	...	...	...	...	-2.37 ± 0.57	...
J10584–107	...						
J18451+063	...	...	-0.745 ± 0.065	-0.83 ± 0.28	-0.81 ± 0.32	...	...
J02022+103							...
J02164+135							-4.57 ± 0.92^{b}
J04403–055	...	...	...	...	...	-19.9 ± 6.6	
J20574+223	...	...	...	...	...	...	0.249 ± 0.041
J22559+057	...	...	...	...	...	...	0.502 ± 0.011
J23064–050	...	...	...	...	...	...	-6.6 ± 1.3^{b}
J01390–179[a]						-12.8 ± 1.5	-5.07 ± 0.39^{b}
J01390–179[a]	-7.8 ± 1.3						
J01390–179[a]	-9.6 ± 1.8	-11.0 ± 1.4	-13.87 ± 0.96	-18.1 ± 1.4	-18.8 ± 1.9	-11.0 ± 1.8	
J04376–024	-1.63 ± 0.30	-1.700 ± 0.24	-2.19 ± 0.44	-1.80 ± 0.26	-2.13 ± 0.72	-1.54 ± 0.27	-1.79 ± 0.20^{b}
J05068–215W	-3.74 ± 0.79	-8.35 ± 0.81	-6.65 ± 0.70	-5.5 ± 1.1	-7.9 ± 1.3	-7.1 ± 1.3	-5.48 ± 0.57^{b}
J08126–215	...	...	...	...	...	...	
J08582+197						-10.6 ± 1.3	-5.48 ± 0.60^{b}
J08589+084	-5.60 ± 0.054					-3.79 ± 0.17	
J10196+198	-2.72 ± 0.32					-5.35 ± 0.79	
J14544+161	-0.70 ± 0.13	-0.87 ± 0.24	-1.19 ± 0.25	-0.92 ± 0.13	-1.21 ± 0.14	-1.13 ± 0.31	-0.84 ± 0.15^{b}
J16554–083N	-1.69 ± 0.31	...	...	...	...	-2.09 ± 0.23	0.258 ± 0.024
J16554–083S	-2.05 ± 0.18					-2.118 ± 0.009	
J18554+084	-1.42 ± 0.25	-2.58 ± 0.34	-2.18 ± 0.38	-1.79 ± 0.34	-2.04 ± 0.27	-2.17 ± 0.24	-1.76 ± 0.28^{b}

[a] Different channels.

[b] Self-absorptions.

Table 13: pEWs of Ca, He and Na lines.

Karmn	pEW [Å]				
	Ca II K	Ca II H	He I D_3	Na I D_2	Na I D_1
J02442+255	-2.60 ± 0.49	-1.49 ± 0.18	...	> 0	> 0
J03133+047	-9.0 ± 2.3	-5.81 ± 0.95	...	> 0	> 0
J04352–161	-6.29 ± 0.47	-1.66 ± 0.27			
J04376–110[a]	-2.86 ± 0.35	-2.24 ± 0.35	...	> 0	> 0
J04376–110[a]			...		
J05068–215E	-17.7 ± 1.1	-7.1 ± 1.2	-0.155 ± 0.013	-0.286 ± 0.020	-0.098 ± 0.014
J06548+332	-4.08 ± 0.60	-1.98 ± 0.41	...	> 0	> 0
J07446+035	-7.16 ± 0.46	-7.54 ± 0.50	-0.678 ± 0.042	-1.148 ± 0.063	-0.613 ± 0.040
J08298+267			...	-3.82 ± 0.29	-1.75 ± 0.11
J08536–034			...	-4.2 ± 1.3	-3.7 ± 1.3
J10289+008	-4.88 ± 0.67	-2.62 ± 0.34	...	> 0	> 0
J10482–113	-17.3 ± 2.4	-13.7 ± 1.6	-0.291 ± 0.014	-6.13 ± 0.26	-3.83 ± 0.16
J10564+070[a]	-42 ± 13	-16.5 ± 4.9			
J10564+070[a]			-1.48 ± 0.37	-4.06 ± 0.65	-2.25 ± 0.53
J11033+359	-1.94 ± 0.21	-1.09 ± 0.15	...	> 0	> 0
J12189+111	...	...	-0.65 ± 0.11	-1.70 ± 0.16	-0.94 ± 0.11
J13005+056	...	...	-0.547 ± 0.022	-1.128 ± 0.090	-0.619 ± 0.036
J13168+170			...	> 0	> 0
J13457+148	-4.43 ± 0.65	-2.84 ± 0.37	...	> 0	> 0
J15598–082	-5.6 ± 1.6	-4.2 ± 1.2			
J16555–083			-0.461 ± 0.082	-5.32 ± 0.80	-4.38 ± 0.75
J17052–050	-3.42 ± 0.63	-3.5 ± 1.6			
J22021+014	-6.76 ± 0.78	-3.57 ± 0.57	...	> 0	> 0
J22532–142	-2.73 ± 0.61	-1.42 ± 0.38	...	> 0	> 0
J22565+165	-5.4 ± 1.6	-4.7 ± 1.3	...		
J04595+017	-13.5 ± 1.5	-9.8 ± 1.7	-0.086 ± 0.008	> 0	> 0
J07403–174	...	...			
J18451+063	-11.6 ± 1.2	-7.8 ± 1.2	...	> 0	> 0
J04403–055	...	...			
J20574+223	-1.36 ± 0.16	-0.85 ± 0.17	...		

Table 13: (continued)

Karmn	pEW [Å]				
	Ca II K	Ca II H	He I D_3	Na I D_2	Na I D_1
J22559+057	-4.39 ± 0.97	-2.64 ± 0.52	...	> 0	> 0
J23064–050	...	...			
J01390–179[a]			-1.56 ± 0.24	-2.86 ± 0.49	-1.58 ± 0.21
J01390–179[a]	-45.1 ± 3.8	-30.5 ± 2.5			
J04376–024	-13.8 ± 3.8	-9.3 ± 2.6		> 0	
J05068–215W	-18.4 ± 2.2	-11.1 ± 1.5	-0.822 ± 0.090	-1.30 ± 0.16	-0.79 ± 0.13
J08126–215	-2.58 ± 0.41	-1.20 ± 0.39			
J08582+197			-0.212 ± 0.010	-2.63 ± 0.16	-1.32 ± 0.17
J08589+084			...	> 0	> 0
J10196+198			-0.476 ± 0.084	-1.230 ± 0.086	-0.741 ± 0.095
J14544+161	-13.7 ± 1.3	-8.88 ± 0.53			
J16554–083N	...	...	...	> 0	> 0
J16554–083S				> 0	> 0
J18554+084	-14.2 ± 1.5	-8.5 ± 1.1			

[a] Different channels.

Table 14: Measured values of $v \sin i$ for our sample.

Karmn	Calibration channel	$v \sin i$ [km/s]	$\Delta v \sin i$ [km/s]	$v \sin i$ "old" [km/s]	Reference
J02442+255	BLU437 (1)	0*		2.5	Browning et al. (2010)
	BLU437 (2)	2.77	0.06		
J05068–215E	RED580 (1)	8.61	0.30	5.3	Reiners et al. (2012)
	RED580 (2)	8.62	0.46		
	RED580 ([a])	8.61	0.25		
J07446+035	RED564	3.97	0.08	4.5	Reiners (2007)
J08298+267	RED564	8.91	0.16	8.1 ± 1.1	Delfosse et al. (1998)
J10482–113	BLU437	0*		3	Mohanty & Basri (2003)
J10564+070	RED564	2.98	0.06		
J11033+359	BLU437 (1)	0*		2.5	Browninget al. (2010)
	BLU437 (2)	0*			
	BLU437 (3)	0*			
J12189+111	RED564	14.59	0.48	9.2 ± 1.9	Delfosse et al. (1998)
J13005+056	RED564	16.43	0.58	16.8	Delfosse et al. (1998)
J15598–082	BLU437 (1)	0*			
	BLU437 (2)	0*			
	BLU437 (3)	0*			
	BLU437 (4)	0*			
J16555–083	RED564	5.50	0.11	9	Jenkins et al. (2009)
J17052–050	BLU437(1)	0*		3	Marcy & Chen (1992)
	BLU437 (2)	0*			
J22021+014	BLU437 (1)	0*		20.21 ± 4.94	White et al. (2007)
	BLU437 (2)	0*			
	BLU437 (3)	0*			
J22532–142	BLU437 (1)	0*		2.5	Browning et al. (2010)
	BLU437 (2)	0*			
	BLU437 (3)	0*			
J04595+017	RED580 (1)	19.40	0.86	14	Torres et al. (2006)
	RED580 (2)	20.54	1.77		
	RED580 ([a])	19.62	0.78		

Table 14: (continued)

Karmn	Channel	$v \sin i$ [km/s]	$\Delta v \sin i$ [km/s]	$v \sin i$ "old" [km/s]	Reference
J20574+223	RED564	10.42	0.43		
J22559+057	RED564	11.57	0.46		
J01390–179	BLU437	29.88	6.54	31.5	Jenkins et al. (2009)
J04376–024	RED580 (1)	15.10	0.46	6.5	Houdebine (2010)
	RED580 (2)	15.44	0.63		
	RED580([a])	15.22	0.37		
J05068–215W	RED580 (1)	2.43	0.11		
	RED580 (2)	5.32	0.24		
	RED580 ([a])	2.93	0.10		
J08126–215	BLU437 (1)	0*		3	Reiners et al. (2012)
	BLU437 (2)	0*			
J08582+197	RED564	16.70	0.64		
J10196+198	RED564 (1)	4.10	0.03		
	RED564 (2)	6.95	0.09		
	RED564 ([a])	4.35	0.03		
J18554+084	BLU437 (1)	22.56	3.55	7.7	Reiners et al. (2012)
	BLU437 (2)	22.76	5.78		
	BLU437 ([a])	22.61	3.03		

* Narrow profiles.

[a] Weighted mean.

Preparation of the carmenes Input Catalogue

Mining public archives for stellar parameters and spectra of M dwarfs with master thesis students

D. Montes[8], J. A. Caballero[10], F. J. Alonso-Floriano[8], M. Cortés-Contreras[8], E. González-Álvarez[8], D. Hidalgo[8], G. Holgado[8], H. Martínez-Rodríguez[8], J. Sanz-Forcada[10] and the CARMENES Consortium[1,2,3,4,5,6,7,8,9,10,11] (http://carmenes.caha.es/)

[1]Max-Planck-Institut für Astronomie • [2]Instituto de Astrofísica de Andalucía • [3]Landessternwarte Königstuhl • [4]Institut de Ciències de l'Espai • [5]Institut für Astrophysik Göttingen • [6]Instituto de Astrofísica de Canarias • [7]Thüringer Landessternwarte Tautenburg • [8]**Universidad Complutense de Madrid** • [9]Hamburger Sternwarte • [10]Centro de Astrobiología • [11]Centro Astronómico Hispano-Alemán – Calar Alto Observatory

We are compiling the most comprehensive database of M dwarfs ever built, CARMENCITA, the **CARMENES Cool dwarf Information and daTa Archive**, which will be the CARMENES 'input catalogue'. In addition to the science preparation with low- and high-resolution spectrographs and lucky imagers (see the other posters at Cool Stars 18), we compile a huge pile of public data on over 2100 M dwarfs, and analyze them, mostly using virtual-observatory tools. Here we describe four specific actions carried out by *master students*. They mine public archives for additional high-resolution spectroscopy (UVES, FEROS and HARPS), multi-band photometry (*FUV-NUV-u-B-g-V-r-R-i-J-H-Ks-W1-W2-W3-W4*), X-ray data (*ROSAT*, *XMM-Newton* and *Chandra*), and periods, rotational velocities and Hα pseudo-equivalent widths. As described, there are many interdependences between all these data.

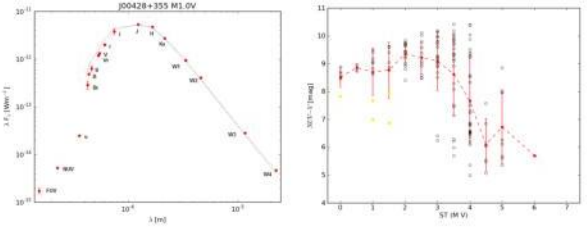

Photometry. *Holgado* compiled photometric data from *GALEX*, SDSS, Tycho-2, UCAC4, CMC14, 2MASS and *WISE* archives for constructing cleansed spectral energy distributions of 158 CARMENCITA stars (*left panel*: SED of FF And) and studying colour-colour relations of 361 bright, late-type, single M dwarfs that surpasses previous works. He also quantified the ultraviolet-excess emission and identified active early M dwarfs (*right panel*: *NUV-FUV* vs. spectral type).

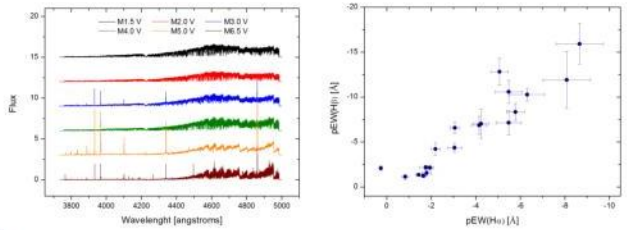

High-resolution spectroscopy. *Martínez-Rodríguez* downloaded 128 UVES spectra of 61 CARMENCITA stars in eight channels (*left panel:* BLU437) and measured pseudo-equivalent widths of Hα−η, Ca II H&K, Na I D1&2 and He I D3. He measured *pEW*(Hα) of 27 M dwarfs for the first time and studied its relation to other lines in emission (right panel: *pEW*(Hβ) vs. *pEW*(Hα)). He also measured *vsini* of 24 stars (7 new) and identified wrong values published in the literature.

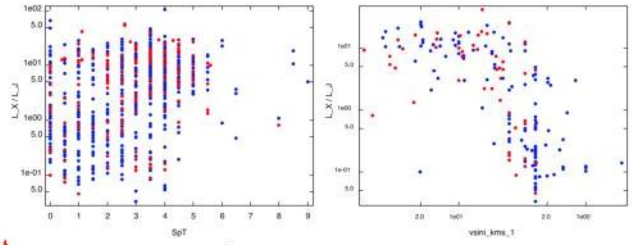

X-ray emission. *González-Álvarez* added new X-ray count-rate and hardness-ratio data of 188 M dwarfs to CARMENCITA. She calculated X-ray fluxes and luminosity ratios L_X/L_J for 770 stars in total and investigated its variation with spectral type (*left panel*) and rotational velocity (*right panel*). She corroborated with a large sample that close binaries (red dots) are more active than single stars and that X-ray saturation starts at *vsini* ≈ 5 km/s.

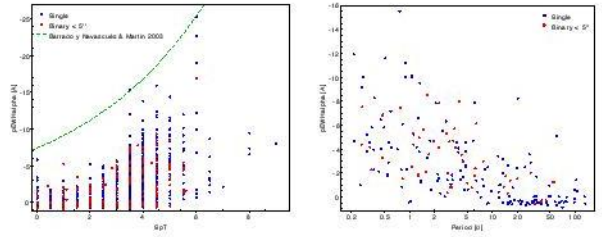

Rotation and activity. *Hidalgo* ransacked dozens of publications and compiled photometric periods for 217 CARMENCITA stars, rotational velocities for 420, pEW(Hα)s for 1766, and membership in young moving groups for 44. He studied the relation between spectral type, Hα activity (*left panel*), close multiplicity, periods (*right panel*) and *vsini*, from where he identified three stars with inclination angles *i* =79.3 to 81.6 deg: DT Vir AB, BD-21 1074 A and FF And.

Unión Europea
Fondo Europeo de Desarrollo Regional
"Una manera de hacer Europa"
MAX-PLANCK-GESELLSCHAFT
CSIC
Calar Alto